We are IntechOpen,
the world's leading publisher of
Open Access books
Built by scientists, for scientists

6,900
Open access books available

186,000
International authors and editors

200M
Downloads

Our authors are among the

154
Countries delivered to

TOP 1%
most cited scientists

12.2%
Contributors from top 500 universities

CLARIVATE ANALYTICS

BOOK CITATION INDEX

INDEXED

WEB OF SCIENCE™

Selection of our books indexed in the Book Citation Index
in Web of Science™ Core Collection (BKCI)

Interested in publishing with us?
Contact book.department@intechopen.com

Numbers displayed above are based on latest data collected.
For more information visit www.intechopen.com

Development of 2″ AlN Substrates Using SiC Seeds

O.V. Avdeev et al.*
Nitride Crystals Ltd., Saint-Petersburg„ 194156
Russia

1. Introduction

The unique properties of the group III-nitrides (Edgar et al., 1999; Jain et al., 2000; Kasap & Capper, 2006) make them the best semiconductor material for

- optoelectronic devices emitting light in the visible and UV spectral ranges (Orton & Foxon, 1998), including sources for general illumination (Craford, 2005; Liu, 2009; Miyajima et al., 2001; Nakamura et al., 2000; Schubert & Kim, 2005; Schubert, 2006; Taguchi, 2003; Zukauskas et al., 2002),

- photodetectors for these spectral ranges, including solar-blind UV detectors,

- high power/high frequency electronic devices capable of operating at high temperatures and in harsh environment (Bennett et al., 2004; Morkoc, 1998; Pearton et al., 2000; Shur, 1998; Skierbiszewski, 2005; Xing et al., 2001).

To fully exploit the potential of the group III-nitrides in optoelectronics and communication technology, two problems are to be solved:

1. difficulties of doping group III-nitrides, especially attaining the high-level p-doping - in 1999 AlN was even called an "undopable" material (Fara et al., 1999) (p-doping is also a problem for other wide bandgap semiconductors - oxides such as ZnO and chalcogenides such as ZnSe;) and

2. the lack of large high crystalline quality native substrates with required electrical properties.

1.1 Substrates for III-nitride devices

The requirements for a good substrate are:

- lateral and vertical[1] lattice matching,

- thermal expansion coefficient (TEC) matching,

---

*T.Yu. Chemekova, E.N. Mokhov, S.S. Nagalyuk (Nitride Crystals Ltd., Saint-Petersburg„ 194156, Russia), H. Helava, M.G. Ramm (Helava Systems Inc., 181 E Industry Court, Site B, Deer Park, NY 11729, USA), A.S. Segal (STR Group - Soft-Impact Ltd., Saint-Petersburg, 194156, Russia), A.I. Zhmakin (A.F. Ioffe Physical Technical Institute, RAS, Saint-Petersburg, 194021, Russia) and Yu.N. Makarov (Nitride Crystals, Inc., Richmond VA 23238, USA)

[1] A vertical lattice mismatch generates additional crystalline defects by upsetting the epitaxial layers, including inversion domain boundaries and stacking faults (Kasap & Capper, 2006).

- chemical compatibility,
- large size ("a size agreeable to an industry" (Schujman & Schowalter, 2010) - at least 2″),
- affordable price.

Sometimes additional features are desirable, e.g., the cleavability for laser diodes or the high electrical resistivity for field effect transistors (FETs).

A substrate determines the crystal orientation, polarity, polytype, surface morphology; the difference in the chemical composition of the substrate and the epitaxial layer could lead to the contamination of the layer with substrate elements.

The lattice mismatch for the semiconductor layer with the lattice constant a is measured by the misfit parameter $f_m = (a - a_s)/a_s$, where a_s is the lattice constant of the substrate. It leads to misfit strain in the grown layer that should be accommodated if the layer thickness exceeds the critical one[2] (according to either the energy minimization theory of Frank-Van der Merwe (Frank & van der Merwe, 1949) or the force balance theory of Matthews-Blakeslee (Matthews & Blakeslee, 1974), see, for example, (Jain et al., 1997; Jain & Hayes, 1991; Zhmakin, 2011b)) via the introduction of misfit dislocations, the modulation of the free surface profile (waviness (Freund, 1995)), the composition modulation (Seol et al., 2003) or the interdiffusion between the layer and the substrate (Lim et al., 2000); formation of the V-grooves and the random stacking faults (Cho et al., 2000) and the mosaic structure of slightly misoriented subgrains in the epitaxial films (Srikant et al., 1997) are also observed. These mechanisms could be cooperative as well as competitive (Hull et al., 2002). In addition to the misfit strain, surface free energies and interface energies are the factors that determine the growth mode (Frank-van der Merve, Stranski-Kristanov, Volmer-Weber, polycrystalline, columnar) (Gilmer et al., 1998; Wadley et al., 2001). Nitride layers grown on the substrates with the large lattice mismatch can also include twin crystals (Matsuoka, 2005; Rojas et al., 1998).

Homoepitaxy provides a better control over the surface morphology and the defect density compared to the heteroepitaxial growth (Cao et al., 2007; Kirchner et al., 1999). The best substrates for GaN-based devices are GaN and AlN. AlN ones are superior for the structures with high Al content, e.g., UV devices (AlN is transparent down to about 200 nm), FETs and both vertical and lateral Schottky and p-i-n diodes (Luo et al., 2002) (unintentionally doped (UID) AlN crystals are insulators[3] in contrast to GaN ones that have a high background

---

[2] The critical thickness is the equilibrium entity, thus metastable metamorphic layers (Hull & Stach, 1996) of higher thickness could exist at low temperatures: e.g., recently an n-type AlGaN layer on the bulk AlN substrate with a thickness more than an order of magnitude greater than the critical value was reported (Grandusky et al., 2009).

[3] The concentration of the residual oxygen is high for the sublimation grown AlN crystals (Herro et al., 2006); however, most of oxygen is incorporated not as a substitutional shallow donor, but as impurity-forming complexes with point and extended defects located deep in the gap (Freitas, 2005; Schultz, 2010; Slack et al., 2002). Below a critical concentration, the presence of oxygen leads to the formation of Al vacancies; at higher concentrations a defect based on octahedrally coordinated Al atoms is formed (Kasap & Capper, 2006).

The effect of the oxygen contamination is more severe on the thermal conductivity of AlN due to the phonon scattering on oxygen defects whose nature does depend on the oxygen concentration (Kasap & Capper, 2006; Kazan et al. , 2006a). For example, the substitutional defect associated with aluminum vacancy serves as a very efficient center for the phonon scattering (Rojo et al., 2001).

concentration of free electrons (Freitas, 2005))[4]. AlN substrates are also the best choice for for nitride-based power devices due to the high thermal conductivity.

The high thermal conductivity of AlN is attributed to the simplicity of the atomic structure, it's low atomic mass, the existence of strong covalent bonding, and low anharmonicity within the lattice (Dinwiddie et al., 1989). Note that the thermal conductivity of AlGaN alloys is smaller than that of pure GaN, to say nothing of AlN, due to the high degree of the disorder in the system (Liu & Balandin, 2005).

The cooling of devices on AlN substrates could be effectively better than of that on SiC substrates that have higher thermal conductivity since the former do not require a buffer layer between the device structure and the substrate that is highly defective and thus presents considerable thermal resistance (Schowalter et al., 2004).

AlN crystals, possessing the highest surface and bulk acoustic wave velocity known for piezoelectric materials, a small temperature coefficient of delay, and a large piezoelectric coupling coefficient, are needed for the surface acoustic wave (SAW) devices[5]. Aluminum nitride for such applications has an evident advantage - AlN crystals could be used up to 1150 °C (Fritze, 2011) (conventional piezoelectric materials are not suited for high-temperature applications, for example, α-quartz αSiO_2 undergoes a phase transformation at 573 °C while lithium niobate $LiNbO_3$ and lithium tetraborate $Li_2B_4O_7$ decompose at 300 °C). AlN crystals are also considered as perspective material for the integration of semiconductor electronic and SAW devices (Cleland et al., 2001).

1.2 Foreign substrates

In the lack of native GaN or AlN substrates, a number of foreign ones are used in practice leading to low quality of the grown epitaxial layers in terms of large threading dislocation density, inversion domain boundaries, partial dislocations bounding stacking faults, bowing of the structure, cracks (Cherns, 2000; Speck, 2001; Speck & Rosner, 1999; Wu et al., 1996; 1998). The near-interfacial region of the film could contain a mixture of cubic and hexagonal GaN (Wu et al., 1996).

The island coalescence is considered as the main mechanism, at least during MBE growth, of the dislocation appearance (Waltereit et al., 2002). Similar conclusion is reached in the study of the early stages of HVPE epitaxy - all the edge and most of the mixed threading dislocation are originated from the island junctions of the high temperature (HT) buffer layer (Golan et al., 1998). An increase of the smoothness was also observed and attributed to the subsequent surface and bulk reconstruction. A strong correlation between the final threading dislocation

---

[4] For example, in GaN crystals grown by the hydride (halide) vapour-phase epitaxy (HVPE) an unintentional n-type conductivity originates from the background doping by silicon and oxygen from the quartz elements of the reactor or from the process gases (Paskova et al., 2010). Fe compensating doping allows one to achieve semi-insulating properties of the layer in this growth method (Vaudo et al., 2003) with the the lowest free carrier concentration reported so far $5 \cdot 10^{13}$ cm^{-3} (Paskova et al., 2009).

However, the performance parameters of AlGaN/GaN heterostructure field-effect transistor (HFET) structure formed by depositing a layer of AlGaN on a relatively thick semi-insulating GaN epitaxial layer are greatly improved by replacing a GaN epitaxial layer with a highly resistive AlN epitaxial layer in the device structure, in particularity, parasitic conduction in the GaN epilayer, leakage current through the GaN epilayer, and the channel electrons spillover into the GaN epilayer have been completely eliminated and the drain current collapse has been reduced (Fan et al., 2006).

[5] Even polycrystal AlN films obtained, for example, by low-cost sputtering are of great interest since the corresponding SAW devices could operate at frequencies above 1GHz (Epelbaum et al., 2004). However, the properties of elasic waves in polycrystal depend on the grain size and orientation.

density in the thick films and the initial island density in the high temperature buffer layer was registered in the MOCVD grown GaN layers on the sapphire substrate (Fini et al., 1998). Early stages of the film growth frequently occur via coherent (dislocation-free) island formation due to the existence of the energy barrier to the introduction of dislocations; dislocations arise at the island edges for large enough islands since those edges are characterized by the large stress (Eisenberg & Kandel, 2002).

A review of the study of the morphology of the heteroepitaxially grown GaN layers using the scanning tunnel microscopy could be found in Ref. (Bakhtizin et al., 2004).

Threading dislocation are electrically active with the charge density of approximately 2 elementary charges per nanometer dislocation length (Müller et al., 2006); surface depressions caused by the high strain-energy density near dislocations are observed on the surface of GaN films (Heying et al., 1999). Edge and mixed (screw/edge) dislocations in nitride materials act as nonradiative recombination centers and as conduits for charge transport resulting in leakage currents and breakdown (Amano et al., 2003; Davis et al., 2002).

While high threading dislocation density is acceptable for light emitting diodes (LEDs)[6] — usually their small effect on the performance is attributed to the potential fluctuations related to the indium composition fluctuations (resulting from the poor In incorporation in the epitaxial layer during the growth or from the phase separation due to the large miscibility gap (I-hsiu & Stringfellow, 1996; Karpov, 1998; Korcak et al., 2007)) observed in the active layers made from the ternary solid solution InGaN and in the corresponding QWs (Christen et al., 2003; Limb, 2007; Mukai et al., 2001) that provide the localization of carriers and reduce their in-plane diffusion to the non-radiative recombination centers — the high dislocation density, however, is fatal for laser diodes and power transistors; even for the LEDs including indium-free violet ones (Usikov et al., 2003) it leads to the drop in the efficiency and is the main factor of the device failure (Karpov, 2009; Roycroft et al., 2004).

The most important foreign substrates are sapphire Al_2O_3 and silicon carbide (6H-SiC or 4H-SiC). The list of other substrates used for group III nitride epitaxy includes GaAs, AlAs, GaP, ZnO, MgO, Mg(Zn) Fe_2O_4, $LiGaO_2$, $LiAlO_2$, SiO_2, $NdGaO_3$, $ScAlMgO_4$, ZrO_2, Mo, glass, quartz glass (Jain et al., 2000; Kukushkin et al., 2008; Miskys et al., 2003).

Sapphire is a good choice for the nitride layers from the crystallographic point of view: crystal orientations of sapphire and gallium nitride grown on c-plane (0001) are parallel, with the unit cell of GaN being rotated by 30° about c axis with respect to the unit cell of sapphire; the $(1\bar{1}00)$ axis of GaN is parallel to the $(12\bar{1}0)$ sapphire axis (Jain et al., 2000).

However, sapphire is inferior (due to the high TEC mismatch and the lattice mismatch being about 15% that corresponds to a critical thickness of less than a monolayer (Jain et al., 2000) compared to 3.5 % for 6H SiC) in the quality of the grown nitride layers leading to higher threading dislocation density.

The insulating nature of sapphire restricts the device architecture, excluding the vertical die design. Bipolar devices fabricated on the sapphire substrates should employ mesa structures with the lateral geometry of the anode and cathode electrodes (with both contacts placed in the same plane) and are especially prone to the current crowding effect - a nonhomogenous in-plane distribution of the current density, especially at the vicinity of the edge of the metal electrodes.

This effect is one of the limiting factors of the efficiency of light emitting diodes, but it is also of concern in other semiconductor devices, e.g., bipolar transistors and Schottky diodes (Chen

---

[6] Threading dislocations with vacancies at Ga sites (Hovakimian, 2009) acting as non-radiative recombination centers (Choi et al., 2004) present more serious problem for GaN/AlGaN system than for GaN/InGaN one (Akasaki & Amano, 2006).

et al., 2007; Paskova et al., 2010). The current crowding can lead to the localized overheating and the formation of thermal hot spots, lowering the internal quantum efficiency of LED and affecting the series resistance of the diode as well as can result in a premature device failure (Bogdanov et al., 2008; Bulashevich et al., 2007; Evstratov et al., 2006).

Another weak point of sapphire as a substrate for the light emitting diodes is a low refractive index of sapphire in comparison to III-nitrides that leads to waveguiding of light emitted in the active region of the LED and thus to the decrease of the light extraction efficiency (Karpov, 2009).

Nevertheless, at present time over 80 % of LEDs are fabricated on sapphire 2″ substrates (Russel, 2006) due to the low cost and availability.

A relatively new approach to the effective use of the sapphire substrates that has been developed for the nitrides light-emitting diodes (LEDs) growth is the nano-patterning of the surface of the substrate: it is expected that the strain induced by the lattice misfits between the GaN epilayers and the sapphire substrates can be effectively accommodated via the nano-trenches (Yan et al., 2007) (the patterning also enhances light extraction from the device (Zhmakin, 2011a)).

A few years ago a possibility to directly obtain aluminum nitride layers on the sapphire by nitriding α-SiO$_2$ surface on large (2 inch) substrate by chemical reaction with N$_2$ - CO gas mixture under carbon-saturation conditions was demonstrated (Fukuyama et al., 2006).

The drawback of SiC substrates is the high cost and the surface roughness on the scale of a few atomic bilayers, leading to a stacking-mismatch defects at the interface between SiC and III-nitride layers in the form of a 2H-polytype (Karpov, 2009; Potin et al., 1998).

Reducing the high cost of SiC substrates while conserving the high thermal conductivity is possible by inserting a thin film of monocrystalline SiC onto polycrystalline SiC (Pecz et al., 2008) which has the thermal conductivity lower than that of single crystal but close to it (Franko & Shanafield, 2004). Polycrystalline SiC is produced by the low cost process of the SiC powder sintering (Medraj et al., 2005). Bonding the thin sapphire layer to polycrystalline AlN (P-AlN) retains the epitaxial template for the growth while improving the thermo-mechanical properties of the substrate (Pinnington et al., 2008). Another example of composite substrates is SiC semiconductor-on-insulator (SOI) structures that are the low cost 3C-SiC (111) substrates fabricated by the conversion of silicon SOI by carbonization of the surface —a reaction with propane and hydrogen at high temperatures (Steckl et al., 1997).

Epitaxy of InGaN/GaN layers on foreign substrates with the large lattice mismatch requires a preliminary growth of a buffer layer or multiple buffer layers (Miskys et al., 2003; Xi et al., 2006). The common example of the use of a double buffer layer is the growth of AlGaN with a starting low-temperature AlN layer on the GaN templates on sapphire which themselves contain the low-temperature GaN buffer layer (Kuwano et al., 2004) or an introduction of an insulating AlN sub-buffer layer on the semi-insulating SiC substrate under the GaN buffer layer (Shealy et al., 2002).

The buffer layer frequently has an amorphous-like structure with small crystallites providing the very smooth morphology (Matsuoka, 2005). AlN is frequently used as the buffer layer material for sapphire and SiC substrates; buffer layers from GaN, AlGaN (including graded AlGaN conducting buffer layers (Moran et al., 2000)), ZnO (Jain et al., 2000; Ougazzaden et al., 2008) or platinum nanocluster (Oh et al., 2009) are used for sapphire while HfN buffer layers for Mo substrates (Okamoto et al., 2009).

The threading dislocation density could be greatly reduced using the lateral epitaxial overgrowth (LEO, the term ELOG is also used) developed in 1990s (Beaumont et al., 1998; Davis et al., 2002; Nam et al., 1997; 1998). This method involves patterning of the substrate

and the initial vertical growth in the "windows" etched in the mask with subsequent growth of material of higher quality laterally over the mask patches. The modification of LEO - the so called pendeo-epitaxy (Davis et al., 2001; Zheleva et al., 1999) - is free of the two major LEO drawbacks (cracking of thick layers and void formation on the top of mask stripes (Wang et al. , 2001)). The crystallographic tilt in the overgrown material is also significantly reduced and the diffusion of impurities from the mask is avoided (Davis et al., 2002).

The extremely low threading dislocation density could be obtained via two sussessive ELO steps with the mask of the second step positioned over the windows etched in the mask during the first step (Pearton et al., 2000).

Growth of GaN or AlN directly on Si surface usually results in the formation polycrystalline films, probably due to the prior formation of amorphous SiN_x layer (Davis et al., 2001a). The large lattice (17%) and TEC (33%) mismatch between Si and GaN cannot be fully accommodated by an AlN buffer layer (Lin et al., 2008), still, involving additionally nitridation (Yamabe et al., 2009) or carbonization of the surface or SiC coating (Kukushkin et al., 2008), some GaN device grown on Si substrates such as HEMTs show an acceptable performance.

In MBE the best results (an order of magnitude decrease of the threading dislocation density in GaN epilayers) are obtained when the growth is initiated by exposing the Si substrate to NH_3 first (Louarn et al., 2009). Usually Si (111) surface (Davis et al., 2001a) is used while an integration with Si microelectronics requires growth on Si (100). In the GaN layers grown on (111) Si substrate inclusions of the cubic nitride phase are frequently observed (Jain et al., 2000).

1.3 Templates & *pseudo bulk* substrates

Considerable efforts were directed to the development of *templates* (the foreign substrates with the deposited thin nitrides layers) (Gautier et al., 2008; Miskys et al., 2003) sometimes referred to as *MOVPE-derived GaN substrates* (Davis et al., 2002) and *pseudo bulk* or *freestanding* nitride substrates (Lee et al., 2004; Nikolaev et al., 2000; Weyers et al., 2008) obtained by separation of the thick nitride layers from the sacrificial substrate after the growth (by laser-assisted lift-off (LLO) (Lee et al., 2004; Paskova et al., 2004) or by etching, e.g, in aqua regia for GaAs substrates) or during the growth on sapphire substrates with patterned GaN seeds by spontaneous self-separation (Tomita et al., 2004).

The quality of the epitaxial layers grown on the templates in comparison to those grown on the basis substrate is under discussion. Recently Ashraf et al. (Ashraf et al., 2008) have used a number of characterization techniques (diffraction interference contrast optical microscopy, scanning electron microscopy, micro-Raman scattering, X-ray diffraction) to asses the quality of the thick GaN layers grown by HVPE directly on the sapphire substrate (with the optimal nucleation layer deposition at low temperatures and low pressures on the nitridated surface) and on the GaN/Al_2O_3 templates prepared by GTS-metalorganic chemical vapour deposition (MOCVD) process (Grzegorczyk et al., 2005) (GTS stands for the gallium treatment step which is a long exposition of the substrate surface to TMGa at high temperature). The authors found that the layers did not significantly differ in the surface morphology and the structural quality, but the layers grown on the MOCVD templates suffered from cracking in few cases while no cracking occurred in the HVPE layers directly grown on sapphire.

1.4 Epitaxial layers and devices on single-crystal native III-nitride substrates

Characterization of AlGaN epilayers with 40 and 50 % concentration of aluminum grown on the single-crystal AlN substrates by Migration Enhanced Metal Organic Chemical Vapour Deposition (MEMOCVD) using the observation of atomic steps in atomic force microscope

scans of epilayers and the measurements of FWHM of X-ray diffraction curves demonstrated an excellent crystallographic quality of the epilayers, the dislocation density of AlGaN layers was estimated to be in mid 10^6cm^{-2} range (Schowalter et al., 2006). The comparison of photoluminescence of the GaN layers deposited on the Al face and on the N face of the single-crystal AlN substrate showed that in the former case photoluminescence is consistent with that of the homoepitaxial Ga-face GaN while in the latter an existance of the tail localized states was found (Tamulatis et al., 2003).

The studies of deep-UV emission of AlGaN quantum wells (Gaska et al., 2002) as well as AlGaN UV (Nishida et al., 2004a; Ren et al., 2007; Xi et al. , 2006a) and InGaN MQW green (Cartwright et al., 2006) LEDs grown on the bulk AlN substrates and blue and UV LED on the bulk GaN substrates (Cao et al., 2004; Cao et al. , 2004a; Du, Lu, Chen, Xiu, Zhang & Zheng, 2010) as well as cyan and green LEDs grown on a-plane (Detchprohm et al., 2008) and m-plane (Detchprohm et al., 2010) GaN bulk substrates prove the superiority of the native substrates, e.g., the luminescence intensity of the quantum well grown on bulk AlN was higher that that of the quantum well grown on SiC by a factor of 28, the noticeable improvement over LEDs grown on sapphire in device impedance and thermal characteristics (Ren et al. , 2007a), the reduction in current-voltage differential resistance and in turn-on voltage (Paskova et al., 2010). The emission spectrum of AlGaN-based UV-LEDs on a bulk AlN substrate under the high current injection is much more stable than that of LEDs fabricated on the conventional substrate (Nishida et al., 2004a;b). Recently J. J. Grandusky et al. have demonstrated mid-UV LED fabricated from pseudomorphic layers on the bulk AlN substrates (Grandusky et al., 2010).

High-quality green (Miyoshi et al., 2009) and violet and near-UV (Perlin et al., 2005) laser diodes have been fabricated on the bulk GaN substrates, in the latter case substrate were grown by the HNPSG.

Studies of high-electron mobility transistors (HEMTs) with the ALGaN channel[7] grown on different substrates also demonstrate the superiority of the single crystal AlN substrates (Hu et al., 2003), in particularity, the use of AlN substrates improved the crystalline quality of the AlGaN layer and lowered the sheet resistance of the 2-dimensional electron gas (Hashimoto et al., 2010).

The substrates cut from the bulk crystals along the specific crystallographic plane can have different orientation (polar, semipolar or nonpolar) (Lu et al., 2008)[8], enhancing the freedom of the device design (Mymrin et al., 2005; Schowalter et al., 2006; Stutzmann et al., 2001): an engineer, using the spontaneous and piezoelectric polarization that is a nonlinear function of the strain and the composition of nitride materials, can tailor the surface and interface charges

---

[7] The channel layer substitution of a wider bandgap AlGaN for a conventional GaN in high electron mobility transistors is an effective method of drastically enhancing the breakdown voltage (Nanjo et al., 2008).

[8] For a long time attempts to grow the nitride epitaxial layers on the nonpolar planes were unsuccessful producing the low quality films (Karpov, 2009). However, recently I. Satoh et al. (Satoh et al., 2010) demonstrated the possibility to fabricate the non-polar AlN substrate by heteroepitaxial growth on m-plane SiC substrates.

Although the dislocation density of the epitaxial layers grown on m-plane was an order of magnitude higher than that on c-plane substrate, the emission intensity was 25 times greater, evidently due to the elimination of the spatial separation of the electron and holes wavefunctions in the quantum wells induced by the built-in polarization field that leads to the decrease of the radiation recombination rate - see, for example, (Chakraborty et al., 2005; McAleese et al., 2006; Ram-Mohana et al., 2006).

High efficiency non-polar m-plane InGaN light emitting diodes and laser diodes have been demonstrated also by M. S. Schmidt et. al. (Schmidt et al. , 2007;a).

to get the desired properties of the heterostructure, for example, to achieve two-dimensional electron gas without modulation doping (Ambacher et al., 2003).

Note that an "effective" cost of single crystal bulk AlN substrates could be rather low if repeated use (removal of the AlN substrate by laser-lift off and recycling[9]) is realized.

The most mature growth technology for bulk group III - nitride crystals is the sublimation growth. Currently, the reproducible growth of large AlN bulk single crystals has been achieved (Bondokov et al., 2008; Helava et al., 2007; Mokhov et al., 2005; Raghothamachar et al., 2006; 2003). Still, a number of problems such as improvement of the crystal seeding and stoichiometry, the reduction of impurities concentration, the maintenance of stable conditions during the long growth remains.

The present chapter reports advances in AlN sublimation growth and its modelling. Both numerical and experimental approaches to understanding and optimization of the sublimation growth of AlN bulk single crystals are reviewed. A developed two-stage technology for the growth of large AlN crystals on SiC seeds that allows to exploit the best features of crucibles made from different materials is described. The superiority of single crystal AlN substrates for the growth of the group-III nitride epitaxial layers and the device performance is demonstrated. The chapter is organized as follows. The next section contains a review of approaches to growth of bulk group III - nitride crystals from liquid - melt or solution - and vapour phases. The sublimation growth of bulk AlN crystals and modelling of this process are considered in the sections 3 & 4, respectively. The developed by the authors two-stage growth procedure based on using SiC seeds and two crucibles made from different materials is described in the section 5. Results of the assessment of the quality of the grown crystals and fabricated single-crystal 2in AlN substrates are presented in the section 6. The section 7 summarizes the results.

2. Growth of bulk group III nitride crystals from liquid and vapour phases

Although the first AlN crystals were synthesized by F. Briegler and A. Gúther using the reaction between molten aluminum and nitrogen about a century and a half ago (see, for example, (Dalmau, 2005; Dalmau & Sitar, 2005) and the small needles of GaN were synthesized by R. Juza and H. Hahn in 1938 by passing ammonia over hot gallium (Jain et al., 2000) (and, similar, the AlN needle crystals were obtained by flowing nitrogen over the compacted AlN powder), growth of bulk GaN, AlN and AlGaN crystals is difficult (Denis et al., 2006); InN bulk crystals have not been demonstrated so far - the thermal instability of the group III - nitride compound increases as one goes down the group III column of the Periodic Mendeleev system (Schowalter et al., 2004).

Bulk group-III nitride crystals could not be congruently grown from the stoichiometric melt under practically acceptable environment conditions (temperature and pressure) as most semiconductors not due to the high melting temperature itself, as sometimes stated, but due to the decomposition of the crystals occurring at much lower temperature resulting from the strong bonding of nitrogen molecule and the low free energy of the crystal (Krukowski,

---

[9] LLO is usually performed to separate group III-nitride structure from the sapphire substrate by a short pulse of UV laser — either the eximer KrF laser at 248 nm or the third harmonic (255 nm) of the Nd:YAG laser — that locally heats the nitride layer causing its decomposition into metal and nitrogen. In case of AlN substrate having a relatively low transparency at short wavelengths an additional operation could be needed — a preliminary thinning of the substrate by chemical etching (Schujman & Schowalter, 2010).

1997)[10]. The congruent melting of gallium nitride has been achieved recently under the severe experimental conditions (the pressure of 6 Gpa and temperature about 2200° C (Utsumi et al., 2003) (so far grown crystals are smaller than 100 μm).

Bulk single group III- nitride crystals could be grown either from solution or from vapour phase. The former is known in three variants: High Nitrogen Pressure Solution Growth (HNPSG), and two "low" pressure techniques — ammonothermal growth and flux growth. Two vapour phase growth methods are halide (hydride) vapour phase epitaxy (HVPE) and sublimation growth. These growth techniques are briefly considered in this section, except sublimation growth that is treated in the next section.

2.1 High Nitrogen Pressure Solution Growth

The solubility of nitrogen in the Ga melt is very low (Nord et al., 2003) and the formation of the N_2 bubbles is possible in the supersaturated GaN liquid (Krukowski, 1997). The nitrogen dissolution in metal melt could be increased by two orders of magnitude —as well known in iron- and steelmaking — by dissolving the nitrogen radicals instead of nitrogen itself, thus ammonia is preferable as an ambient gas (Kawahara et al., 2005).

The growth of the centimeter-size GaN crystals was achieved at high temperatures and ultra-high N_2 pressures that provide a sufficient concentration of nitrogen in the Ga melt (High Nitrogen Pressure Solution Growth - HNPSG) (Grzegory, 2001; Porowski & Grzegory, 1997). The GaN crystals grown by this method have a very low threading dislocation density of $10^2 cm^{-2}$. Similar temperature and pressure are used in the Pressure-Controlled Solution Growth - PCSG (Denis et al., 2006). The HNPSG without an intentional seeding produces the needle-like AlN crystals (Bockowski, 2001). Both needle-like and bulk form of AlN single crystals up to 1 cm and 1 mm, respectively, were grown at high nitrogen pressure of the order of 1 GPa and temperatures up to 2000 K (Bockowski et al., 2001).

Recently (Al,Ga)N bulk single crystals have been grown from the Al/Ga melt under high nitrogen pressure (up to 10 kbar) at high temperature (1425 - 1780 °C) with an aluminum content from 0.22 to 0.91 (Belousov, 2010; Belousov et al., 2010; 2009). The largest crystal was $0.8 \times 0.8 \times 0.8$ mm^3. The distinct feature of this study is the use of pre-reacted polycrystalline (Al,Ga)N or AlN pellets. The composition of the growing crystal was controlled by the proper choice of the pressure and temperature.

Note, however, that the high-pressure requirement limits the scalability of the HNPSG to the growth of small area crystals.

2.2 Ammonothermal growth and flux growth

The extreme parameters needed for the HNPSG and the PCSG are reduced in the ammonothermal (Purdy et al., 2003; Yoshikawa et al., 2004) and the alkali metal flux methods (Aoki et al., 2002; Onda et al., 2002; Song et al., 2003; Yano et al., 2000). The former is similar to the well-known hydrothermal growth of quartz crystals (Iwasaki & Iwasaki, 2002) (that closely reproduces the growth of amethyst in nature (Carter & Norton, 2007)) with supercritical ammonia instead of water. This method belongs to a wide class of methods called *solvothermal*, another member of this class of growth techniques is *glycothermal* growth from glycerinated solutions (Adekore et al., 2006; Callahan & Chen, 2010). Being a low-temperature

---

[10] For example, the melting point of GaN is 2300° C at the pressure of 6GPa; at lower pressure GaN dissociates into metallic gallium and nitrogen gas or a state where nitrogen is dissolved in liquid gallium (Ohtani et al., 2007); at atmospheric pressure GaN decomposes at 1150 K (Ehrentraut & Fukuda, 2008).

process, solvothermal growth minimize the incidence of the temperature-induced point defects.

The relatively low growth rates of the solvothermal methods are partially compensated by the ability to grow multiple crystals (for example, over a hundred in the case of ZnO and over a two thousands in the case of quartz) in a single run.

Hundreds of different compounds are grown by the hydrothermal method, some of them at ambient conditions such as aluminum potassium sulfate and potassium dihydrogen sulfate (KDP). Hydrothermal growth of the low-defect ZnO crystals requires a high oxygen overpressure (about 50 atm) (Nause & Nemeth, 2005), but thus far remains a unique example of the industrial growth of widebandgap semiconductors by the solvothermal method (Ehrentraut et al., 2006).

In solvothermal method a liquid polar solvent (water in hydrothermal and ammonia in ammonothermal growth) forms metastable intermediate products with the solute (nutrient). Mineralizers are needed to increase the solubility of the nutrient.

No growth of GaN crystals is observed in the pure Ga solution. It is necessary, similar to other hydrothermal-type processes, to add either lithium as a transporting agent or either acidic or basic *complexing agents - mineralizers* (Callahan & Chen, 2010) such NH_4X (where X= Cl, Br, I) (Purdy et al., 2003; Yoshikawa et al., 2004) or gallium triiodide with CuI or LiI (Purdy et al., 2003). In the first approach chemical reactions occur in the solution involving such compounds as $LiGa(NH_2)_2$ and $LiNH_2$. Acidic mineralizers effectively increase the reaction rate by increasing the amount of anions in the solution. A mixture of alkali metal amide and iodide has been successfully used in (Ketchum & Kolis, 2001) while neither of these mineralizers alone could provide GaN growth. The growth mechanism involves formation of the intermediate soluble Ga-imide complex. For the growth of AlN crystals a Ca_3N_2 or Na flux has been used (Yano et al., 2000).

In the sodium flux method Na acts as a catalyst that releases electrons easily. It is speculated that nitrogen in N_2 molecule absorbed onto the Ga-Na melt surface receives electrons from Na, that weakens the N_2 bonds and causes the dissociation of N_2 into two negatively charged radicals at much lower temperature and pressure (Aoki et al., 2002). The use of lithium instead of sodium is more promising since the ability of the former to fix nitrogen is higher and that allows one to achieve the growth of GaN single crystals under the pressure of 1-2 atm (Song et al., 2003).

The sodium flux growth is performed in either a closed or in an open tube (Aoki et al., 2002; Onda et al., 2002). In the former the only source of nitrogen is a solid precursor such as NaN_3 powder, thus the pressure decreases during the process as nitrogen is being consumed for the GaN growth. In the latter N_2 or its mixture with NH_3 serves as a nitrogen source and the pressure can be either kept constant or varied with the time by a prescribed law (Onda et al., 2002). NH_3 is superior over N_2, however, the size of GaN crystals grown in $NH_3 - N_2$ mixture is smaller then in pure N_2.

Cathodoluminescence spectra show that the GaN crystals grown in the open system are of higher quality (Aoki et al., 2000). Sometimes the formation of the intermetallic compound $Ga_{39}Na_{22}$ is observed (Aoki et al., 2000). Black color of grown crystals is explained either by the nitrogen deficiency or by the oxygen impurity (Aoki et al. , 2002a; Aoki et al., 2000).

Change of the crystal shape from prismatic to platelet with increasing the Na/(Na+Ga) ratio has been studied in (Aoki et al., 2000; Yamane et al., 1998). An agglomeration of small crystals at high values of this ratio is explained by the drastic increase of the supersaturation. It can lead to the growth instability due to the constitutional supercooling similar to processes in pure Ga melt HNPSG (Grzegory, 2001; Grzegory et al., 2002). Polycrystallization occurs in the

seeded growth when the pressure exceeds the threshold value for the unseeded nucleation (Iwahashi et al., 2003). The growth rate of GaN crystals is anisotropic being higher in c direction. Usually N-polar face is smooth while Ga polar face is rough, corrugated with macrosteps (Frayssinet et al., 2001; Skromme et al., 2002). However, the reverse pattern could also be observed (Yamane et al., 1998) probably due to the impurity incorporation: in (Grzegory, 2001) the growth instability has been observed on the Ga-polar face without doping and on the N-polar face in the presence of Mg.

It is speculated (Grzegory et al., 2002) that the nucleation rates at the different faces can vary greatly due to the different geometry of the 2D nuclei (hexagonal or square, differing in the number of atoms in the nucleus as well as the number of the broken bonds). In the Li flux method (Song et al., 2003) liquid gallium infiltrates into porous Li_3N and reacts to produce $GaLi_3N_2$ and metal Li. In the case of the excess of Li_3N no growth of GaN has been observed and only $GaLi_3N_2$ has been formed. The authors consider two possible mechanisms of GaN growth - direct reaction of $GaLi_3N_2$ with gallium and dissolution of $GaLi_3N_2$ in Li-Ga melt to form ternary system - and conclude that the latter is the one that is most probable.

The growth rate of GaN in the ammonothermal technique is rather small (not greater than 2μ/hour (Fukuda & Ehrebtraut, 2007)). Frequently a columnar growth occurs yielding the crystals of poor quality (Waldrip, 2007; Wang et al. , 2001a). Still, "tremendous progress over the last decade" has been recently reviewed in (Avrutin et al., 2010; Ehrentraut & Fukuda, 2010). It is claimed that since the ammothermal growth occurs at near thermodynamic equilibrium with the extremely low supersaturation, the high crystalline quality can be expected (Ehrentraut & Kagamitanii, 2010). However, the growth of the large GaN crystals by the ammonothermal method using the HVPE-grown free-standing substrates gives disappointing results: the density of dislocations in the grown crystals are two order of magnitude larger than in HVPE seed (Callahan & Chen, 2010; Ohtani et al., 2007).

A new method called Electrochemical Solution Growth (ESG) based on the transport of the nitrogen ion N^{3-} in the molten chloride salt is being developed now (Waldrip, 2007); so far only millimeter-size GaN crystals were produced. A reaction between Ga and Li_3N under NH_3 atmosphere via the formation of $LiNH_2$ is used to grow GaN crystals by T. Hirano et al. (Hirano et al., 2009).

The ammonothermal growth of polycrystalline Aln at temperatures between $525°$ and $550°$ in alkaline conditions (using potassium azide KN_3 as the mineralizer) was reported by B. T. Adekore et al. (Adekore et al., 2006). The thickness of the layers grown on the GaN seed in 21 days varied from 100 to 1500 μm. For the growth of AlN crystals a Ca_3N_2 or Na flux has been used (Yano et al., 2000). The growth using AlN wires as a starting material shows the very high contamination of oxygen, probably due to the intrinsic oxidized Al surface. Precipitation of single crystalline AlN from Cu-Al-Ti solution was studied in (Yonemura et al., 2005). The larges pencil type crystal has 3mm in length and 0.2 mm in its diameter. An AlN platelet (1.5 mm diameter) was also obtained by the regrowth technique. Evidently, the solution growth of AlN cannot be developed in a near future to the production scale due to the difficult control of process and low growth rate.

The alkali metal flux growth has been used in the liquid phase epitaxy (LPE) (Kawahara et al., 2005). 3 μm-thick MOCVD-GaN layers with the threading dislocation density $1.3 \cdot 10^6$ were used to grow the 500 μm crystals that were almost dislocation free. PL intensity of the LPE-GaN with Na flux and Ca-Na mixed flux was 47 and 86 times, respectively, greater than that of the seed crystal. LPE was also used to grow the hexagonal or prismatic platelets at ambient pressure with NH_3 as a nitrogen source; the growth anisotropy was found to be

comparable to that in bulk Na flux growth and much smaller than in HNPSG (Meissner et al., 2004).

2.3 Halide (hydride) vapour phase epitaxy - HVPE

A HVPE reactor consists of the two main zones: the source zone where chloride gas of group III metal is formed and the growth zone where it is mixed with NH_3 to grow the nitride crystal. This method, including its variant *iodine* vapour phase epitaxy (IVPE) (Cai et al., 2010), and corresponding mathematical models are well documented (see, in addition to the just cited chapter, for example (Dmitriev & Usikov, 2006; Hemmingsson et al., 2010; Segal et al., 2009) and the references therein), thus only a few comments are in order here.

The uniqueness of HVPE is the applicability of this method to both growth of thick substrates and epitaxial heterostructures due to an extremely wide range of growth rates (1 - 150 μm/hour), the low cost compared to the MOCVD, an ability to grow the heavily doped p-layers, an absence of the carbon contamination.

At present, however, the freestanding AlN films grown by HVPE are of inferior crystalline quality: the typical value of the x-ray rocking curve Full Width at Half Maximum (FWHM) is at least an order of magnitude larger than that of AlN substrate cut out from bulk AlN boule (Cai et al., 2010; Freitas, 2010); the self-separated thick (85 μm) AlN films grown recently by the three-step modification of HVPE that include the formation of numerous voids at the interface between an AlN layer and the sapphire substrate has the dislocation density on order of 10^9cm^{-2} (Kumagai et al., 2008); the sublimation-grown bulk AlN crystals usually are transparent while the HVPE-grown ones are opaque (Cai et al., 2010), Tabl. 37.16.

The reverse breakdown voltage of the m-i-m structure on bulk AlN was an order of magnitude greater than that on free-standing GaN (Luo et al., 2002) proving high potential of Al-Ga-N system for high power rectifiers.

3. Sublimation growth of AlN crystals

Sublimation[11] (also *sublimation - recondensation*) growth (or physical vapour transport - PVT) of AlN is the most mature technology of the bulk nitride crystal growth (Dalmau & Sitar, 2005; 2010) (sublimation is also used to grow AlN fibers (Bao et al., 2009) and other nitride compounds, for example, the titanium nitride crystals (Du, Edgar, Kenik & Meyer, 2010); sublimation growth of GaN crystals is less successful (Kallinger et al., 2008)[12]). Probably the first application of PVT is the growth of the single cadmium sulfide crystals more than a half of a century ago.

The growth of other wide bandgap materials such as ZnO using physical vapour transport also was reported (Rojo et al., 2006). Note that the earlier attempts to grow ZnO by sublimation were performed using much lower temperatures and the sublimation activators such as H_2O,

---

[11] "Sublimation" refers to the direct formation of the vapour from the solid phase; however, usually it is implicitly assumed that solid and vapour are the same substance. Thus the use of this term for the process in question is not strictly correct: AlN does not *sublime* but rather *decomposes*.

[12] Evidently, the source of the problem is the nitrogen pressure over GaN surface that is six orders of magnitude higher than that over AlN (Freitas, 2010).
The gallium vapour is generated either from the molten gallium or by the thermal decomposition of the GaN powder (Waldrip, 2007). In order to suppress the dissociation of GaN, NH_3 gas is used in addition to nitrogen. It is possible to grow only pellets of GaN with the size up to several square millimeters due to the depletion of the source (Ohtani et al., 2007). There was a great interest in this method in 1960s and 1970s that has been lost due to the great progress in producing pseudo-bulk GaN substrates by HVPE.

$HgCl_2$ or ZnX_2 (where X = Cl, Br or I) gases so that both sublimation and growth involve reversible chemical reaction (Rojo et al., 2006).

The simplest case for the analysis is the so called congruent (diffusionless) vapor transport (Abernathy et al., 1979): sublimation at the source and condensation at the growing crystal surface are congruent (i.e. there is no change in the composition), no foreign gases are involved and the vapour stoichiometry is preserved across the growth facility. Thus there is no relative motion of the vapour components - the diffusion plays no role, the transport is provided by the "Stefan wind" ("drift transport" (Karpov et al., 1999)) and the growth rate is maximal (Brinkman & Carles, 1998). An experimental path to the "Dryburgh" regime is the decreasing the pressure in the reactor (Wolfson & Mokhov, 2010). The growth rate under the "vacuum" conditions (the growth cell was placed in a special container with a background pressure maintained at the level about 10^{-4} Torr) corresponds to the growth rate in nitrogen atmosphere at temperatures about 350–400 K higher (Karpov et al., 1999).

In the other extreme case where inert gas is the predominant component in the vapour, the growth rate is directly proportional to the partial pressure difference at the source and at the crystal. Polycrystalline AlN frequently is grown by the sublimation method with the grain size increasing and the number of grain per unit area decreasing in the first few mm of growth (Noveski et al., 2004b).

The overall reaction of AlN sublimation growth can be written as

$$(AlN)_{\text{solid}} \xrightarrow[T_{growth}+\Delta T]{Sublimation} Al_{vapour} + \frac{1}{2}N_2 \xrightarrow[T_{growth}]{Deposition} (AlN)_{\text{solid}}$$
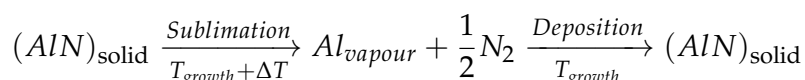
This method developed by G.A. Slack and T.F. McNelly in 1976 (Slack & McNelly, 1977) (whose largest crystal was 10 mm long by 3mm diameter) now provides the growth rates up to 1 mm/hr (Rojo et al., 2002)) and the high crystal quality (the threading dislocation density is lower than 1000 cm² and FWHM of the rocking curve is less than 10 arcsec in the best samples (Raghothamachar et al., 2003)).

Either a spontaneous nucleation (a self-seeding growth) without any attempt to control the crystal orientation or an intentional seeding (homoepitaxial (Hartmann et al., 2008) or heteroepitaxial (Lu, 2006; Miyanaga et al., 2006)) can be exploited. The SiC substrates are often used (Lu et al., 2008; Mokhov et al., 2002), other substrates —sapphire, tantalum carbide (TaC) and niobium carbide (NbC) —also have been tried (Lee, 2007).

The decomposition of SiC at high temperature affects the growth morphology and could provoke the growth of polycrystalline AlN (Noveski et al., 2004a). Fig. 1 clearly shows the graphitization of the SiC substrate (silicon evaporation) propagating from its lower side.

Both the crucible and the source usually are cylindrical, however, the conical crucibles are used sometimes (Slack & McNelly, 1977) as well a central hole in the powder source to increase the source surface area (Wang et al., 2006).

In contrast to the bulk SiC sublimation growth, there is no evidence of the polytypism in the bulk AlN wurtzite 2H polytype structure that has the lowest formation energy (Bondokov et al., 2007).

The high growth temperature and the highly reactive Al vapour create a problem in selection of crucible material that should have melting point well above 2300 C, a reasonable degree of chemical compatibility with AlN, relatively low vapor pressures, and the relatively small thermal expansion coefficient (Slack et al., 2004).

Different crucibles have been tried including ones made from refractory transition metals (W, Ta, Nb, Zr) and graphite coated with SiC, NbC or TaC (Dalmau & Sitar, 2005; Lu, 2006) revealing their weak points: e.g., the boron nitride growth environment results in the highly
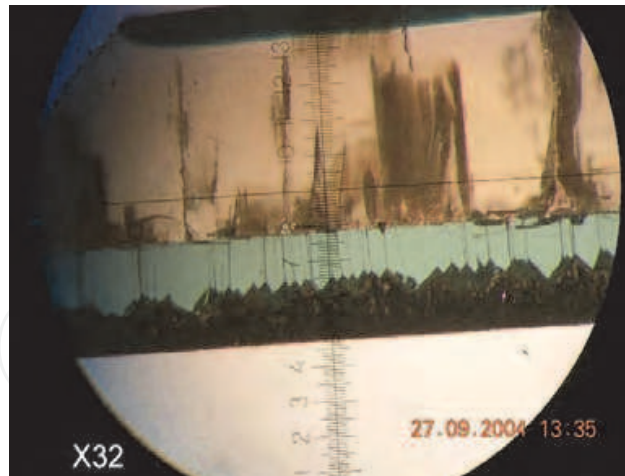
Fig. 1. Graphitization of the SiC substrate during AlN growth.

anisotropic growth (Dalmau & Sitar, 2005), the coated graphite crucibles deteriorate at high temperatures and carbon detrimentally influence the growth morphology as in the pure C crucibles; the crucibles made from nitrides or carbides suffer severe cracking. Among the most successful ones are the crucibles made from transition metals and their carbides (Lu, 2006).

The nature of other components of the growth facility such as heating elements along with the crucible material defines an environment that is responsible for the crystal contamination with different impurities (compatibility of the reactor materials has been considered, among others, by B. Epelbaum et al. (Epelbaum et al., 2002) and C.M. Balkas et al. (Balkas et al., 1997)).

The duration of growth process is limited by the degradation of the crucible (de Almeida & Rojo, 2002; Wang et al., 2006) and of the graphite insulation (Cai et al., 2006) as well as by continuous operation of the source that requires the temperature gradients within the source to be as low as possible (Bogdanov et al., 2003; 2004).

The growth temperature influence the size of AlN nuclei (Yazdi et al., 2006) and thus the crystal morphology (Sitar et al., 2004). The dislocations in the crystal can arise both during growth or after the growth in the course of the thermomechanical stress relaxation (Bogdanov et al., 2003; Klapper, 2010; Kochuguev et al., 2001; Zhmakin et al., 2000). The effect of substrate misorientation and buffer layers on growth modes and defects in AlN sublimed onto 6H-SiC substrates were studied in Refs. (Shi et al., 2001), (Yakimova et al., 2005); different growth modes were related to the low mobility of AlN adatoms on the crystal surface.

The grown bulk AlN crystals (the typical growth rate is about 100 μ/hour) usually have the rough side surface while the top surface could be facetted. The crystals are transparent with colour from yellow or amber to glass-clear (Fig. 2) having the Bragg FWHM 60 - 150 arc sec (Helava et al., 2007).

The reddish samples turned out to contain Fe^{2+} impurity (Ilyin et al., 2010). The below band-gap absorption bands limiting UV transparency are attributed to the point defects (Bickermann et al., 2010), for example, the band-to-impurity absorption manifesting itself as yellow coloration is thought to be related to either the doubly negative charged state V_{Al}^{2-}, the isolated aluminum vacancies $(V_{Al})^{3-/2-}$ (Hung et al., 2004; Sedhain et al., 2009) or the Al vacancy-impurity complexes (Lu et al., 2008).

(a) (b)

(c)
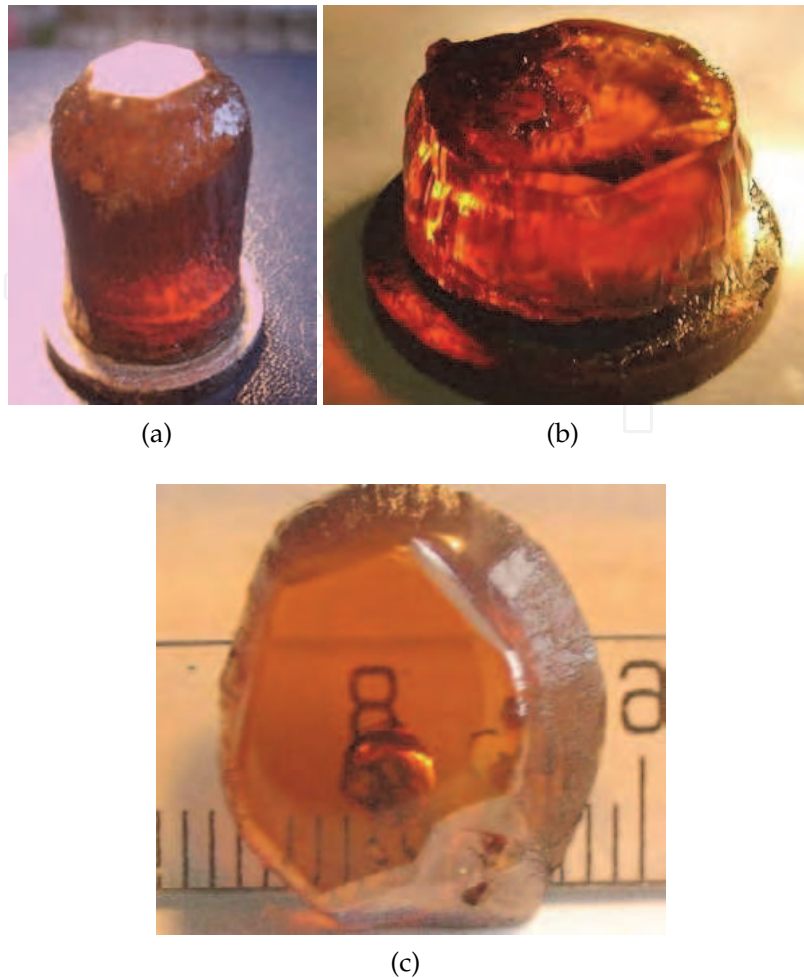
Fig. 2. Examples of grown bulk AlN crystals.

4. Modelling of bulk AlN growth

Since the AlN sublimation growth is implemented in a tightly closed crucible under high-temperature, it is difficult to study and control the growth process *in situ*, thus the importance of the mathematical modelling is evident (Bogdanov et al., 2003; 2004; Chen et al., 2008; de Almeida & Rojo, 2002; Ern & Guermond, 2004; Wellmann et al., 2006; Wu et al., 2005; Zhmakin, 2004).

The aims of numerical simulation are to explain and to predict the growth behaviour. Numerical simulation is not a substitute for experiment, but a complement to it. Numerical models can provide detailed information on the flow, temperature and concentration fields, strain in the crystals etc. which can be measured experimentally only partly or not at all. On the other hand, numerical models depend on experimental data (materials properties, boundary conditions and so on). Moreover, numerical predictions are unreliable unless models are validated using experimental data in the widest possible range of macroscopic parameters.

"Modelling" and "Simulation" are frequently used as synonyms. In Computational Fluid Dynamics (CFD) community, however, the former usually refers to the development or modification of a model while the latter is reserved for the application of the model (AIAA, 1998).

A model should relate the process specification (equipment geometry, materials properties and transport coefficients, technological parameters such as the heating power and heater position, external electromagnetic fields, orientation of the growth facility etc.) to its outputs: crystals yield, crystal quality, process duration and production costs.

If one needs a single criteria (ideally, quantifiable) to estimate the practical usefulness of the simulation, the best choice is probably the reliability of a computer prediction (Oden, 2002). It should be stressed, however, that this parameter characterizes not the model itself, but the simulation, being depending on the adequacy of the model and the accuracy of the computations as well as on the particular aim of the simulations. Evidently, the same results could be considered successful if one is interested in unveiling some trend - and unsatisfactory if the goal is to find, for example, the exact position of the inductor coils in the growth furnace. The straightforward use of the model is referred to as a direct problem (see Table 1).

Process Specification		Process Output
Equipment geometry Materials properties Process parameters	$\Longrightarrow$ Direct (Insight) $\Longleftarrow$ Inverse (Optimization)	Growth rate Crystal quality Process duration Production costs

Table 1. Simulation scheme

From a practical point of view the reversed formulation is more useful: how one should change the equipment design or the process parameters to improve the crystal quality or to reduce production costs, for example. The simplest way is a "try-and-error" approach: to use one's intuition to introduce changes into the process specification or into the growth facility design/size, perform simulation and evaluate results. Sometimes, especially at the early development stages, an even simpler "blind search" (Luft et al., 1999) approach is exploited which essentially is a screening of a range of parameters.

A more systematic way is to state an inverse problem by indicating

1. which geometry characteristics of the reactor or operating conditions (control parameters) could be varied and

2. what criteria should be used to measure the success of the optimization.

The *inverse* problems are, unfortunately, ill-conditioned (*not-well-posed*) and their solution requires some kind of a regularization (Tihonov & Arsenin, 1977) that frequently is just the restriction on the space of possible solutions.

Mathematical models, as well as numerical methods, used for simulation of crystal growth are essentially the same as in other Computational Continuum Mechanics (CCM) applications (heat transfer, fluid dynamics, electromagnetics, elasticity). Both the block-structured and the unstructured grids are used to solve practical problems.

The advantage of the unstructured grids is the relative ease with which the complex geometry can be treated. This approach needs the minimum input description of the domain to be discretized and is not tied closely to its topology in contrast to the block-structured grid. The required CPU time to attain the prescribed accuracy may be less than for the block-structured approach due to the much lesser total number of the grid cells as a direct sequence of the second advantage of the unstructured grids — the easiness of an adaptive mesh refinement, which allows one to place the cells exactly where needed.

The main difference between simulation of the thin film growth and the bulk crystal growth is that in the former case the computational domain can be considered fixed due to the small

thickness of the epitaxial layer. Numerical study of the bulk crystal growth requires the use of either the moving grids or a regeneration of the grid. The latter approach is attractive when one can exploit a quasi-stationary approximation of the growth processes (the characteristic time of the crystal shape changes is large compared to the hydrodynamic/thermal time).

A simulation of the crystal growth requires solution of the conjugated multidisciplinary problem. The key sub-problem is the computation of the fluid flow coupled to the global heat transfer in the growth facility. Frequently, the global solution is used to the specify boundary conditions for a smaller imbedded computational domain where a more elaborate physical model is considered.

4.1 Low-Mach number (hyposonic) equations

The low-Mach number Navier–Stokes equations seem to be the most adequate model for gas flows with essentially subsonic velocities and large temperature variations (Makarov & Zhmakin, 1989). These equations provide the results identical to the full compressible Navier–Stokes computations while reducing greatly CPU time. Often (when gas mixtures used are not diluted) a CFD problem can not be decoupled from the mass transfer one (Egorov & Zhmakin, 1998).

The hyposonic flow equations follow from the full compressible Navier–Stokes equations under the following assumptions (Makarov & Zhmakin, 1989):

1) the Mach number is small $M^2 \ll 1$;
2) the hydrostatic compressibility parameter $\varepsilon = gL/R_g T_0$ is small $e \ll 1$;
3) the characteristic time τ is large compared to an acoustic time scale $\tau \gg L/a$

and for N_s-species mixture flows may be written in the following vector form:

$$\nabla \cdot \rho \mathbf{V} = 0$$
$$\nabla \cdot \left(\rho \mathbf{V} \mathbf{V} + p\hat{I} - \hat{\tau} \right) - \left(\rho - \rho_0 \right) \mathbf{g} = 0$$
$$\nabla \cdot \left(\rho \mathbf{V} h + \mathbf{q} \right) = 0$$
$$\nabla \cdot \left(\rho \mathbf{V} c_s + \mathbf{J}_s \right) = W_s \, , \ s = 1, 2, \ldots, N_s$$

where ρ is the mixture density, $\mathbf{V}$ is the mixture mass-averaged velocity, h is the mixture specific enthalpy, c_s is the mass-fraction of s-th species, p is the dynamic pressure, τ is the viscous stress tensor, $\mathbf{q}$ is the heat flux, $\mathbf{J_s}$ is the mass diffusion flux of the s-th species.

The constitutive relations required to close the system are the state equations for the perfect gas mixture with the variable specific heat:

$$\rho \frac{R}{m} T = p_0 = const \, , \ 1/m = \sum_{s=1}^{N_s} \left(c_s / m_s \right)$$

$$h = \sum_{s=1}^{N_s} c_s h_s(T) \, , \ h_s(T) = h_s^0 + \int_{T^0}^{T} Cp_s(T) dT$$

and the relations for the molecular transfer fluxes: the viscous stress tensor

$$\hat{\tau} = -\frac{2}{3} \mu \left(\nabla \cdot \mathbf{V} \right) \hat{I} + \mu \left(\nabla \mathbf{V} + \mathbf{V} \nabla \right)$$

the heat flux

$$\mathbf{q} = -\lambda \nabla T + \sum_{s=1}^{N_s} h_s \mathbf{J}_s + p_0 \sum_{s=1}^{N_s} k_s^T \mathbf{J}_s / (\rho c_s)$$

and the diffusion flux of sth component

$$\mathbf{J}_s = -\rho D_s \left(\nabla c_s + \frac{m_s}{m} k_s^T \frac{\nabla T}{T} \right)$$

Generally both homogeneous and heterogeneous chemical reactions are to be taken into account, the latter resulting in the highly nonlinear boundary conditions.

4.2 Conjugate heat transfer

The steady-state temperature distribution inside the solid block without heat sources satisfies the scalar equation of thermal conductivity:

$$\nabla \cdot (-\lambda_{solid} \nabla T) = 0$$

The heat conduction is the simplest heat transfer mechanism. Still, two aspects of heat conduction in crystal growth problems should be mentioned.

Firstly, one needs to account for the anisotropic thermal conductivity for certain crystals and for the solid blocks manufactured from the pyrolytic graphite. In the first case the degree of the anisotropy, being determined by the crystal composition and the crystallographic symmetry, is usually not large. The pyrolytic graphite is obtained by the pyrolysis of hydrocarbon gas at high temperature in the vacuum furnace and has a layered structure with the highly ordered hexagonally arranged carbon atoms in planes and the randomly oriented atoms in the perpendicular direction. The ratio of the values of the thermal conductivity in the different directions is 100-400, depending on the material quality.

Whether anisotropy forces one to consider a three-dimensional problem for the geometrically two-dimensional configuration depends on the crystal symmetry and the orientation of its principal axes. For example, if the symmetry axis coincides with the [0001] axis of a hexagonal crystal such as SiC, the solution should be isotropic with respect to rotations around the axis and the two-dimensional formulation is valid.

Secondly, some parts of the facility could be modelled as the porous medium. Powder source is used in a number of techniques such as the metal flux method for growth of bulk GaN crystals from Li-Ga-N liquid phase (Song et al., 2004), the ammonothermal method for GaN (Yoshikawa et al., 2004), the sublimation growth of single crystals of wide bandgap semiconductors (SiC, AlN) (Bogdanov et al., 2003; Dhanaraj et al., 2003). The granular or fibrous medium is often used for the insulation. The usual approach in the computation of the global heat transfer in the facility is to treat the porous media using the effective thermal conductivity. For a given porous structure this quantity is a function of the pressure and the temperature that determine the relative contribution of the solid matrix conduction, heat conduction through the medium (gas) filling the pores and radiation to the total heat transfer. Experimental data being rather scarce, especially at high temperatures, the main problem is to formulate a model that could adequately extrapolate the effective thermal conductivity beyond the measured range of the pressures and temperatures (Daryabeigi, 1999; Kitanin et al., 1998). The effective thermal conductivity could be two orders of magnitude smaller than that of bulk material that is evidently favorable for the use of the porous media as insulation. However, it has a detrimental effect on the optimal heating of the SiC powder source in the

sublimation method (Kitanin et al., 1998). The composition, the porosity and the thermal conductivity of the SiC powder vary during the growth process (Karpov et al., 2001a).

Often radiative heat exchange through a non-participating fluid between solid surfaces can be accounted for under the assumption of the gray-diffusive surface radiation. All solid blocks are assumed to be opaque, while the external boundaries of the gaseous domain may be semi-transparent. Computation of the total radiative flux incoming to the given small surface element requires knowledge of the configuration factors (view factors). Calculation of these view factors via an integration over the complex geometry of the emitting area with account for the shadowing effect is described in details in (Dupre et al., 1990). If the view factors are known, the total radiative flux incoming to the surface element $i(i = \overline{1, N_e}$, where N_e is the total number of surface elements on the boundary) can be calculated as a sum

$$q_i^{in} = \sum_{j=1}^{N_e} q_j^{out} F_{ij},$$

where q^{in} and q^{out} are the radiation fluxes to the wall and from the wall, F_{ij} are the view factors. For the semitransparent external boundary the radiative flux out from the objects inside the region could be calculated by the Stefan-Boltzmann law and definitions of emissivity (E), reflectivity (R) and transmissivity (T) as

$$q_I^{out} = \sigma E_i T_I^4 + R_i q_I^{in} + T_I \sigma T_a^4,$$

where σ is the Stefan-Boltzmann constant and T_a is the ambient temperature.

4.3 Boundary conditions

Boundary conditions at the surfaces where heterogeneous reactions occur are formulated under assumptions that growth is limited by mass transport to the surface, the properties of the adsobtion layer are identical to those of the solid phase and are described by the following equations:

total zero flux of the inert gas

$$\rho u c_0 + J_0 = 0$$

equations relating the total species fluxes and the rates of the heterogeneous reactions

$$\rho u c_i + J_i = M_i \sum_{r=1}^{N_r} \nu_{ir} \dot{w}_r , i = 1, \ldots, N_k^r$$

the mass action law

$$\prod_{i=1}^{N_k^r} X_i^{\nu_{ir}} = K_r , r = 1, \ldots, N_r$$

the normalization condition

$$\sum_{i=0}^{N_k^r} X_i = 1,$$

where N_k^r is the number of the gas phase species participating in the surface reactions, subscript "0" refers to the inert ('carrier') gas, N_E is the total number of elements, N_S is the number of solid state phases, $N_r = N_k^r - N_E + N_S$ is the number of reactions, ν_{ir} is the stoichiometric coefficient of ith component in rth reaction, $\dot{w}_r$ is the rate of rth heterogeneous

reaction, u is Stephan velocity, c_i and M_i are mass concentration and molar mass of ith component, J_i is the normal diffusion flux of ith component, K_r is the equilibrium constant of rth heterogeneous chemical reaction.

When experimental data on the reaction constants are absent, their values could be estimated using thermodynamic properties of individual materials as

$$\ln K_r = \frac{1}{RT} \sum_{i=1}^{N_k^r + N_s} \nu_{ir} G_i - \ln\left(\frac{p_s}{p}\right) \sum_{i=1}^{N_k^r} \nu_{ir},$$

where G_i is the Gibb's potential of the Ith component at normal pressure.

Theoretical analysis of AlN PVT growth was probably first performed in (Dryburgh, 1992). In this paper, the surface decomposition of low-reactive nitrogen was noticed as the rate-limiting stage of the AlN evaporation/ growth. kinetic mechanism. An one-dimensional model of the process was developed, no transport effects being taken into account. In contrast, most of the later studies assumed the AlN growth rate to be limited by the species transport (Noveski et al., 2004b; Wu et al., 2004) and the AlN growth rate was found using the Hertz-Knudsen equation for the interface Al fluxes at the AlN surfaces. Under the additional assumption of a low Al content in the vapor, an approximate explicit relationship for the AlN growth rate was derived.

These studies, unfortunately, neither clarified the boundaries of the kinetically- and transport-limited approximations nor accounted for the mass exchange between the crucible and the ambient through the small gaps and/or through the porous crucible walls that may essentially affect the process. Besides, they do not consider the evolution of the AlN crystal and of the source and the corresponding gradual change of the growth conditions. The evolution effects are also important as they determine the crystallization front shape that, in turn, affects distributions of dislocations and other defects in the crystal (a slightly convex crystallization front is preferable). A model of AlN sublimation growth that does not rely on the kinetically or transport limited approximations and describes all the above effects within a single approach was developed in (Karpov et al., 2001; Karpov et al., 1999; Segal et al., 2000) where an one-dimensional stationary model was considered.

The developed evolutionary model for AlN growth relies on the following assumptions:

• there are only Al and N_2 species in the gas phase (volatile impurities are negligible);

• the growth rate of the AlN crystal is determined by the local vapor composition and temperature but independent of the surface orientation (the isotropic growth);

• the evaporation of the AlN source occurs from the surface only (dense polycrystalline sources is used rather than porous sources);

• the evolution of the AlN source and the crystal occurs much slower than the transfer processes (the quasi-stationary transfer).

The model of AlN sublimation growth is based on the conventional description of heat and radiation transfer, gas flow dynamics, and species diffusion in the growth system coupled with the reduced quasi-thermodynamic description of the surface kinetics at the AlN surfaces. The latter was earlier applied to the modelling of other growth techniques (see, for example, (Segal et al., 2004) and references therein). As applied to AlN sublimation growth, it utilizes the extended Hertz-Knudsen relationships (Segal et al., 1999) for two reactive gaseous species, Al and N_2

$$J_i = \alpha_i(T)\beta_i(T)(P_i^w - P_i^e)$$

Here, J_i are the interface molar fluxes, $\alpha_i(T)$ are the temperature-dependent sticking probabilities,

$$\beta_i(T) = (2\pi\mu_i RT)^{-1/2}$$

are the Hertz-Knudsen collision factors, μ_i are the molar masses, R is the gas constant, P_i^w are the species partial pressures at the interface, P_i^e are the quasi-equilibrium (thermodynamic) species pressures, and subscript i indicates a particular species (Al or N_2).

The Al sticking probability is assumed unity due to its high reactivity. In contrast, the N_2 sticking probability is very low. In (Karpov et al., 2001), it was fitted as a function of temperature using data of (Dreger et al., 1962) on the AlN evaporation in vacuum (more recent data of (Fan & Newman, 2001) confirmed the derived approximation)

$$\alpha_{N_2}(T) = \frac{3.5 \exp -30000/T}{1 + 8 \cdot 10^{15} \exp 55000/T}.$$

The pressures P_i^e satisfy the mass-action law equation

$$(P_{Al}^e)^2 \, P_{N_2}^e = K(T),$$

where $K(T)$ is the equilibrium constant for the surface reaction

$$2Al + N_2 \Leftrightarrow 2AlN(s)$$
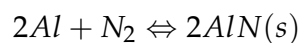
The model was validated in (Segal et al., 2000) by the comparison with the experimental data on the AlN growth rate as a function of the temperature and the pressure; it is implemented as software package Virtual Reactor^{TM} (Bogdanov et al., 2001; STR-soft, 2000). Virtual Reactor^{TM} provides an accurate simulation of all major physical-chemical phenomena relevant to this method such as resistive or RF heating ; conductive, convective and radiative heat transfer; mass transfer in gas and porous media; heterogeneous chemical reactions at the catalytic walls and on the surface of powder granules; deposits formation; formation of elastic strain and dislocations in the growing crystal; the evolution of the crystal and of the deposit shape, including partial facetting of the crystal surface. The problem is solved using a quasi-stationary formulation.

Temperature distributions in the tungsten and in the graphite furnaces for PVT growth of 2 inch diameter AlN boules are shown on Figs. 3, 4, respectively.

Computations revealed, in particularity, that the growth characteristics are extremely sensitive to the temperature distribution in the crucible, for which reason an accurate prediction of this distribution is of primary importance for successful modeling. Figure 5 illustrates the high accuracy of temperature prediction.

Good agreement with experimental data proves the adequacy of the model. The small deviation of the points and the curve is probably due to some uncertainty in the thermal and optical properties of the materials involved at high temperatures.

The distribution of the Al vapor molar fraction in the gaps between the AlN source (bottom), the seed (top), and the walls of the carbonized tantalum crucible in the graphite furnace is shown on Fig. 6.

If the growth occurs in a hermetically closed and chemically inert crucible, the inside static pressure is spontaneously established to provide the conservation of the initial difference between the total numbers of aluminum and nitrogen atoms in the crucible. This quantity is constant since the moment of the sealing of the crucible because the vapour-solid mass

(a) Temperature distribution in the tungsten (b) Temperature profile
furnace   along the axis of the
                                                                     tungsten crucible
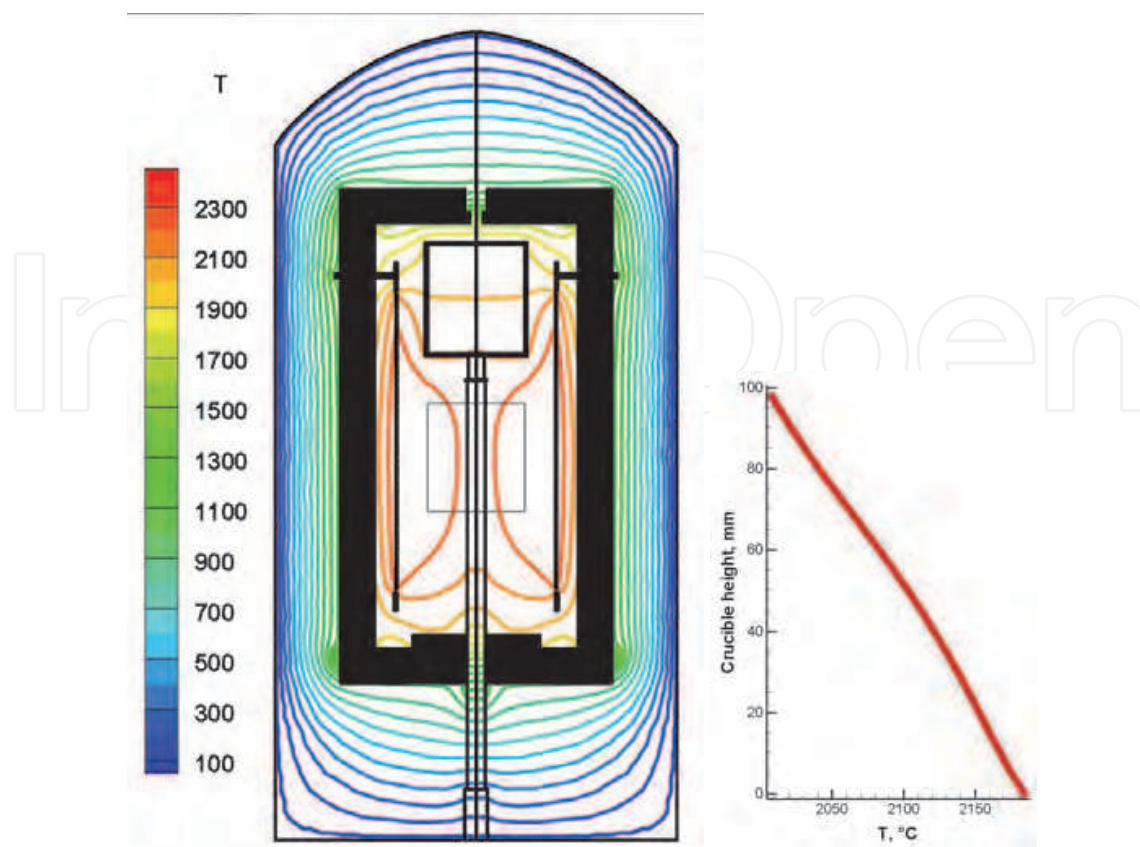
Fig. 3. Temperature distribution in the tungsten furnace.

exchange occurs stoichiometrically (at the AlN surfaces) or does not occur at all (at the inert crucible' walls). l
Due to the existence of the small gap between the crucible body and lid, the ambient pressure strongly affects the growth process, which is largely related to the notion of critical pressure. In equilibrium

$$J_i = 0$$
$$P_i^e = P_i^w$$

and the partial pressures of the two species can be found from the system of two equations:

$$(P_{Al}^w)^2 P_{N_2}^w = K(T)$$
$$P_{Al}^w + P_{N_2}^w = P,$$

where P is the total pressure in the crucible. Analysis shows that if

$$P > P^\star(T) = 3/2[2K(T)]^{1/3}$$

with $P^\star$ denoting the critical pressure, then the system has two solutions corresponding to the Al-rich and N-rich vapor. Since the vapor composition in the crucible is established due to
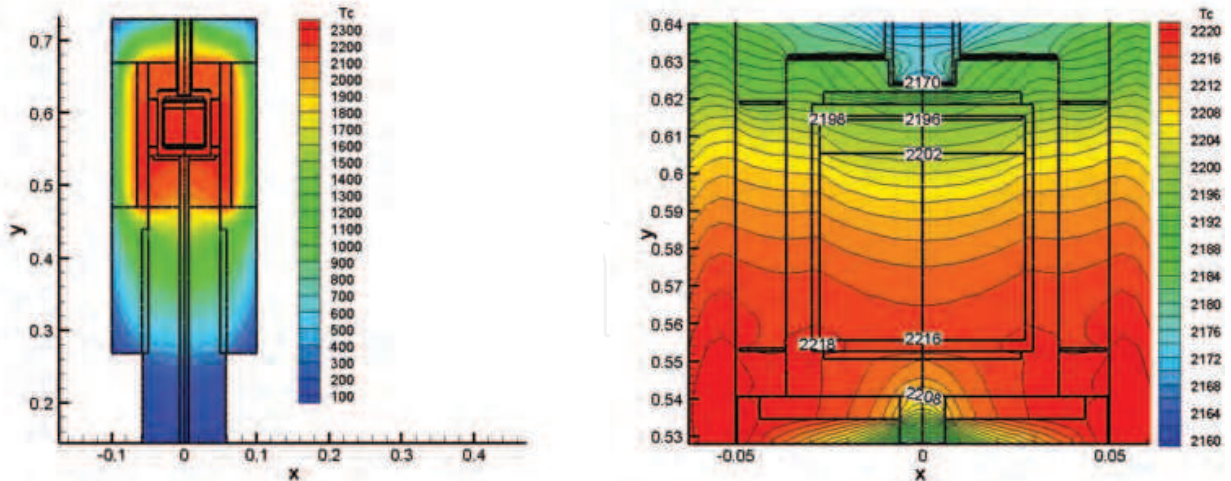
(a) Temperature distribution in the graphite furnace (b) Temperature distribution in the carbonized tantalum crucible

Fig. 4. Temperature distribution in the graphite furnace.
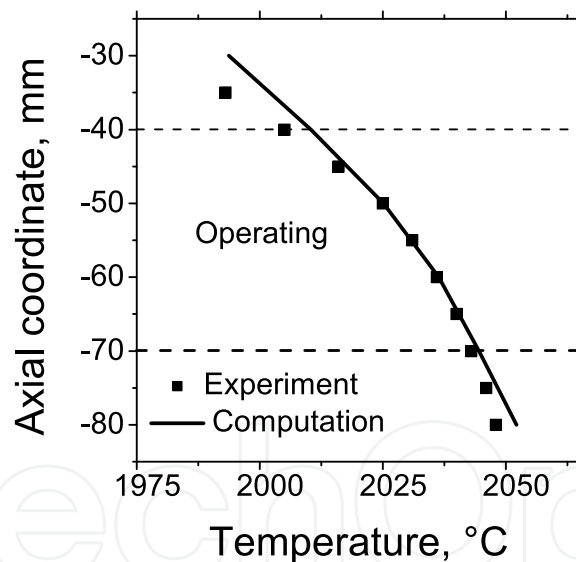
Fig. 5. Temperature at the center of the crucible lid vs. crucible coordinate at the vertical axis, computed (solid line) and pyrometrically measured (points).

mass exchange with the nitrogen ambient, the N-rich branch should be selected. If $P = P^\star(T)$, then there is the unique solution corresponding to the stoichiometric vapor, and if $P < P^\star(T)$, there is no solution. The latter means that in a hermetically closed crucible the equilibrium pressure is always higher than the critical pressure.

In a non-hermetic crucible, the equilibrium is impossible if the ambient pressure is so low that the related pressure inside the crucible is lower than the critical pressure. In this case, both the AlN source and seed evaporate, with the Al/N_2 vapor coming out from the crucible
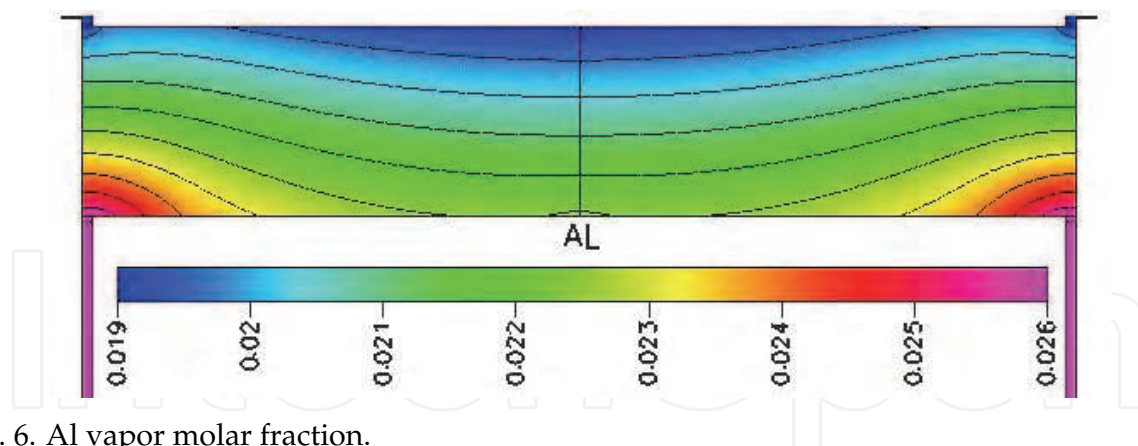
Fig. 6. Al vapor molar fraction.

to the ambient (see Fig. 7 where the pressure inside the crucible and AlN crystal growth rate vs. ambient pressure are shown for different gaps between the side crucible wall and the lid). Mass exchange between the crucible and the ambient occurs through a narrow
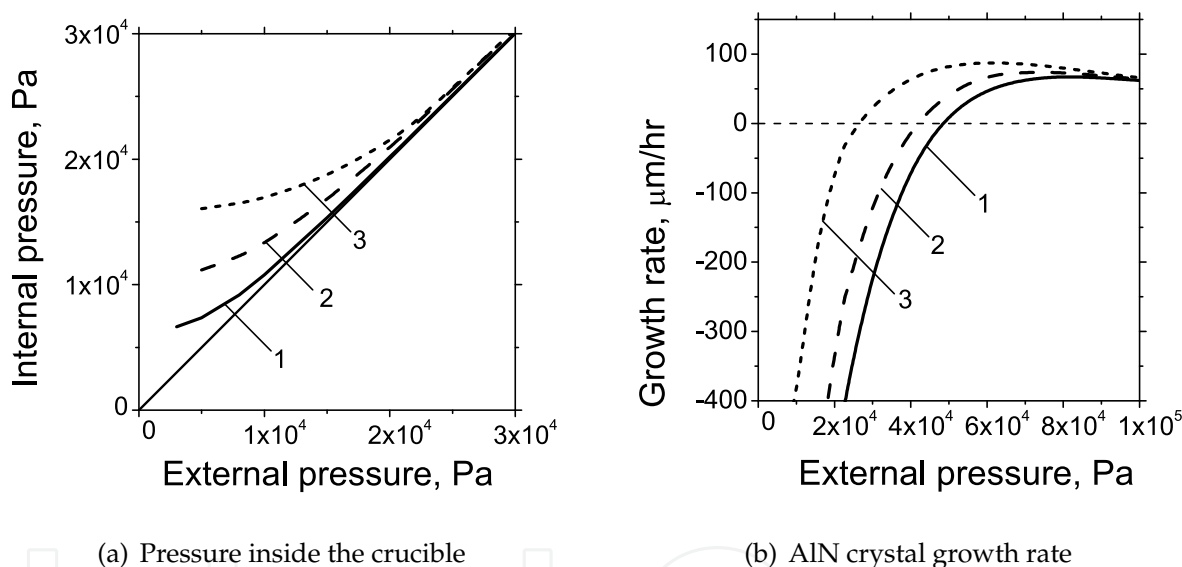
(a) Pressure inside the crucible   (b) AlN crystal growth rate

Fig. 7. Pressure inside the crucible (a) and AlN crystal growth rate (b) vs. ambient pressure at different gaps between the side crucible wall and the lid: 1 - gap length λ is 1 mm, gap thickness δ is 100 μm, 2 - $\lambda = 1$ mm, $\delta = 50\mu m$, 3 - $\lambda = 10$ mm, $\delta = 100\mu m$.

ring gap between the crucible side wall and the lid. The internal and external pressures are close to each other at a sufficiently high external pressure but considerably deviate as it decreases, depending on the gap hydraulic resistance ζ that is proportional to the gap length and inversely proportional to the third power of the gap thickness. Al and N_2 evaporate from the AlN source and then either deposit on the AlN crystal or escape from the crucible. The ratio of the deposited and escaped material depends on the external pressure and on ζ. Figure 7 shows the computed dependencies of the AlN growth rate on the ambient pressure at the crystal center.

As the external pressure decreases, a higher fraction of the material escapes from the crucible and the growth rate decreases. At a sufficiently low ambient pressure P_a^0, the crystal begins

evaporating, with all vapors coming out from the crucible through the gap (negative growth rates). The value P_a^0 decreases with the gap hydraulic resistance (at a sufficiently high ζ, the crystal does not evaporate at an arbitrary small ambient pressure). The local AlN evaporation/growth rate is determined by the local supersaturation, both for the source and seed. The local interface flux on an AlN surface can be approximated as

$$J \approx \frac{\left(P_{Al}^w\right)^2 P_{N_2}^w / K(T) - 1}{4/[3\beta_{Al}(T)P_{Al}^w] + 1/[3\alpha_{N_2}\beta_{N_2}(T)P_{N_2}^w]}$$

Here, the quantity in the numerator is the local supersaturation that represents the driving force for the local AlN evaporation/growth while the denominator corresponds to the local kinetic resistance. The distribution of the supersaturation over the crystal surface determines its evolution (Fig. 8). Black lines with arrows are the streamlines, gray lines are the

(a) Computations   (b) Experiment
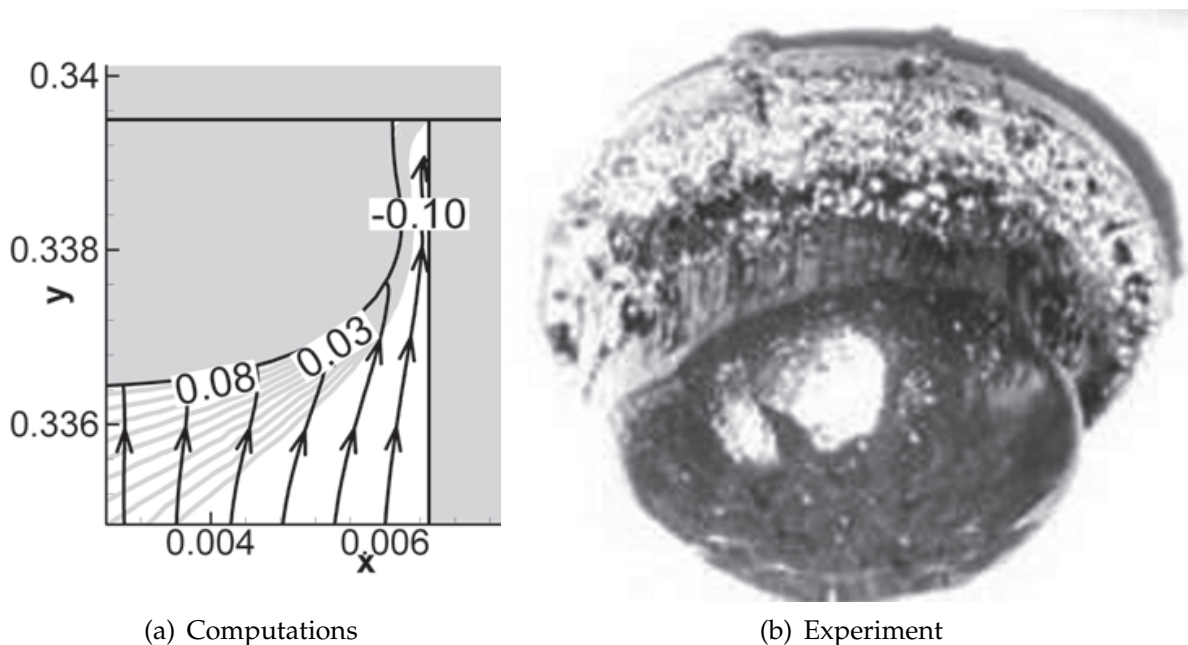
Fig. 8. Shape of AlN boule after 20 hrs of growth.

supersaturation isolines, numbers at the crystal surface are the local supersaturation values. Note that the absolute values of supersaturation are rather small due to the smallness of the relative temperature difference between the source and the seed.

The higher the local supersaturation is, the faster the crystal grows there. At the very periphery, supersaturation is negative due to the species exchange between the crucible and the ambient through the ring gap (here, the vapor is enriched by N_2 and depleted in Al) and the crystal evaporates, taking a mushroom shape; the vapor escapes from the crucible through the gap (the last right streamline is directed to the gap). Computational results are in good agreement with the observed crystal shapes. Using this model, we have optimized the growth conditions and crucible design, which eventually favored the growth of 2″ diameter and up to 10 mm long AlN boules with a slightly convex shape providing a low defect content in the crystal.

5. Experimental set up for AlN bulk growth

Before AlN seeds become available, SiC (4H and 6H of both (0001)C and (0001)Si orientations (Mokhov et al., 2002)) seeds were used. SiC has a small *a*-lattice mismatch with AlN - 0.96% for 6H-SiC and 1.2% for 4H-SiC. However, SiC substrates are known to degrade at high temperatures required for the AlN growth.

A two-stage technology to exploit the best features of different crucibles by avoiding interaction of W with Si and C that form easily melted eutectics and by limiting the incorporation of Si and C in C-rich environment was applied (the AlN crystals grown on SiC seeds in C-containing ambient contain a lot of Si and C impurities that, in particularity, determine the color of the crystal):

1. seeding and initial growth of the 2-3 mm long AlN crystals on the SiC seeds in the TaC crucibles in graphite equipment and

2. growth of bulk AlN crystals on the AlN seeds in tungsten crucibles and equipment.

High-quality AlN seeds of large diameter are currently unavailable while use of AlN seeds of a smaller diameter requires long multi-time lateral overgrowth of the crystals to reach the desired diameters, as the lateral overgrowth angle was found not to exceed 10-15 degrees — the diameter enlargement of AlN boules is often associated with defect generation (Bondokov et al., 2006) or the crack formation (Schujman & Schowalter, 2010).

Another kind of the two-stage procedure was reported by M. Strassburg et al. (Strassburg et al., 2004) where the temperature was gradually ramped between the two stages and by Z. Sitar et al. (Sitar et al., 2004) who used vaporization of Al (use of the metal vapour source is called *direct synthesis method* by K. Nishino et al. (Nishino et al., 2002))[13] at the first and the AlN powder source at higher temperature at the second stage; two-stage growth was also used by R. Dalmau et al. (Dalmau et al., 2005) with stages differing in the growth temperature and, thus, growth rate.

5.1 Pre-growth processing

Preparation of W crucibles includes annealing of W ones to remove the adsorbed impurities, while for Ta crucibles a pre-carbonization is necessary (Fig. 9). These crucibles are remarkably thermally and chemically stable and can endure over 3000 hours of the cumulative AlN growth in graphite (tungsten) equipment.

The presence of oxygen is detrimental in AlN growth due to the formation of oxynitrides and enhanced formation of stacking faults (de Almeida & Rojo, 2002; Majewski & Vogl, 1998) that can induce shallow electronic states (Northrup, 2005) and decrease the thermal conductivity. Oxygen has a negligible effect on the growth rate itself, but it can, at low temperature (e.g., during the heating of the system), provoke generation of Al_2O_3 inclusions (Karpov et al., 2003) that, in turn, causes surface roughness (Kazan et al., 2006). The addition of the hydrogen to the nitrogen during growth is beneficial (Karpov et al., 2001); alternatively, the sources could be processed to reduce the oxygen content. The source of oxygen in the sublimation AlN growth is the hydroxides and oxides on the surface of AlN particles (Edgar et al., 2008).

High-purity AlN sources were prepared from the commercially available AlN powders either by the annealing in the N_2 atmosphere or by the sublimation-recrystallization (Epelbaum

---

[13] Such method provides a high growth rate (5 mm/hour) but the long-term growth is impossible due to the formation of a nitride layer over the metallic Al source and resulting drop of the Al vapour pressure (Lu, 2006).

Fig. 9. Ta (dark gray) crucible (diameter 63 mm) completely covered with a layer of TaC-Ta$_2$C ceramics (gold) that is converted into TaCN during the growth to prevent the formation of easily melted eutectics (Ta-Si and Ta-Al) (Vodakov et al., 2003).

et al., 2004; Helava et al., 2007), producing, respectively, dense porous or polycrystalline AlN source[14].

The content of impurities in the AlN samples was studied using glow discharge mass spectrometry (GDMS). Sublimation-recrystallization was found to be superior and accepted as a standard technique.

SiC seeds were cut from 6H SiC bulk crystals as 0.5 mm thick round plates of different diameters (15-50 mm). The SiC seeds are mechanically lapped and mounted onto the crucible lid using the C-based glue. The technique of the lateral overgrowth of AlN crystals from small-diameter AlN seeds can also be attempted starting from 0.5 mm thick and 15-18 mm diameter AlN seeds from previously grown AlN bulk single crystals. These seeds are similarly mechanically processed and mounted onto the crucible lid with the AlN-based glue.

---

[14] In a two-step procedure developed by L. Du & J.H. Edgar (Du & Edgar, 2010) the low temperature (< 1000 °C) annealing was followed by a high temperature (> 1900 °C) sintering aimed at the reduction of the specific surface area of the AlN powder through the particle agglomeration. Sintering could be applied not only to raw AlN powder, but also to the flakes obtained by pressing the AlN powder (Han et al., 2008).

Evidently, the initial contamination of the AlN powder depends on the process of its synthesis. AlN powder is usually obtained either by the carbothermal reduction of Al$_2$O$_3$ or by direct nitridation of metals, both methods having very long reaction times (hours or even days) - see (Radwan & Miyamoto, 2006) and references therein. The recently proposed microwave-assisted synthesis with addition of ammonium chloride to produce HCl as an intermediate product requires much shorter time - tens of minutes (Angappan et al., 2010). Another fast method is the combustion of ultrafine aluminum powder in air; in this case additives could increase the yield of AlN (Gromov et al., 2005).

5.2 Seeding and initial growth

Use of SiC seeds in pre-carbonized Ta crucibles in graphite RF-heated furnaces is necessarily accompanied by the diffusion of Si and, to a lesser degree, of C into AlN. This process along with the lattice and TEC mismatch results in generation of defects at the SiC-AlN interface, such as micropipes inherited from SiC, dislocations, cracks, and others. Thus in-house sublimation grown *thick* low dislocation density (dislocation etch pits density $1\text{-}4\cdot10^3 cm^{-2}$ after 30 min etching in molten KOH) micropipe-free SiC substrates (60 mm in diameter) have been used (Fig. 10). X-ray diffractometry and topography of the grown AlN layers show that
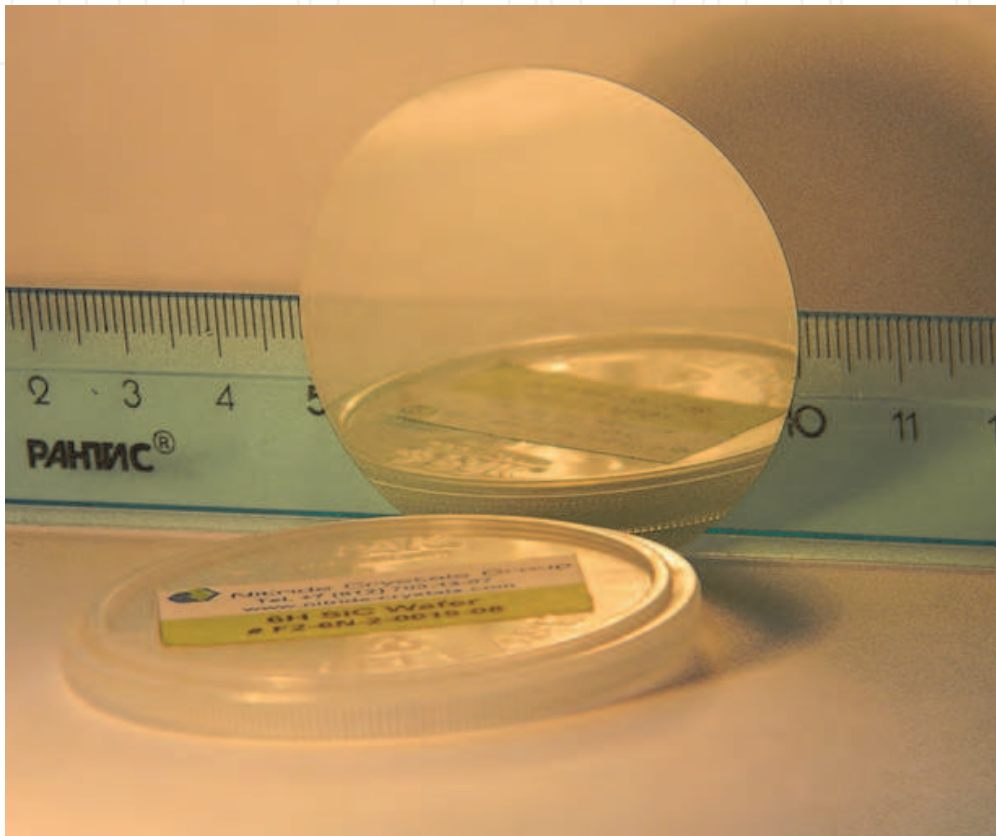
Fig. 10. Thick micropipe-free 2in SiC substrates.

FWHMs of the rocking curves in ω-scan to lie in the range of 60-120 arcsec. At the same time, the c-parameter of the crystal lattice is found to vary as 4.984-4.988 A, which suggests that the AlN layers contain much impurity (the reference value of the c-parameter for pure AlN is 4.982). X-ray microanalysis with SEM shows 5-6% wt of Si and 1% wt of C in the AlN layers. Concentration of other impurities is less than 100 ppm.

It is known that the typical temperature of AlN growth on SiC seeds is lower by 200-300 °C than that on AlN seeds for the comparable growth rates (Epelbaum et al., 2001). Analysis of the three-phase thermodynamic equilibrium in the system Al/N/Si/C(vapor)-AlN(solid)-SiC(solid) allows finding gaseous species that may be responsible for the more intensive AlN growth on SiC. Calculation of the equilibrium partial pressures of the most volatile species in this system (more than 30 gaseous species were considered) showed that there are two "cross" volatile species (AlNC and Si_2N) that may intensify AlN growth on SiC.

5.3 Growth of bulk AlN crystals starting from AlN seeds

The 2-3 mm thick AlN layers (Fig. 11) are separated from the SiC substrate and mounted on the tungsten crucible lid with the AlN-based glue. AlN bulk crystals 10-20 mm long are

Fig. 11. 2in AlN seed grown on 60 mm micropipe-free SiC substrate.

grown in the W crucibles in the W resistively heated furnace (Mokhov et al., 2005), the growth temperature was varied in the range of 2050-2250 °C, the N_2 pressure was varied in the range of 0.5-1 atm, and the AlN growth rate was of 50-150 μm/hr. Long AlN crystals grow for several dozens of hours and often in several runs.

The evolution of the crystal quality via the improvement of the growth regime from the 2-inch diameter 10 mm long bulk AlN crystal having a single-crystal core of about 40 mm diameter and a polycrystalline rim (Avdeev et al., 2010; 2011) to the "good enough" single crystal (and, hence, the substrate) is illustrated by Fig. 12.

6. Properties of sublimation-grown AlN

Currently the technology provides stable reproducible growth of up to 2″ diameter and 10-15 mm long AlN single crystals. Post-growth processing includes calibration, slicing into wafers, mechanical lapping-polishing, finishing chemical-mechanical polishing (CMP) to remove the subsurface damage due to the mechanical polishing that extends up to 4000 Å below the surface (Chen et al., 2008; Freitas, 2005), and characterization.

Impurities such as oxygen, silicon, carbon, boron contribute to the absorption and emission bands below the bandgap (Senawiratne et al., 2005) and thus reduce the AlN transparency in the UV spectral range. The content of impurities in the AlN seeds grown on SiC substrates
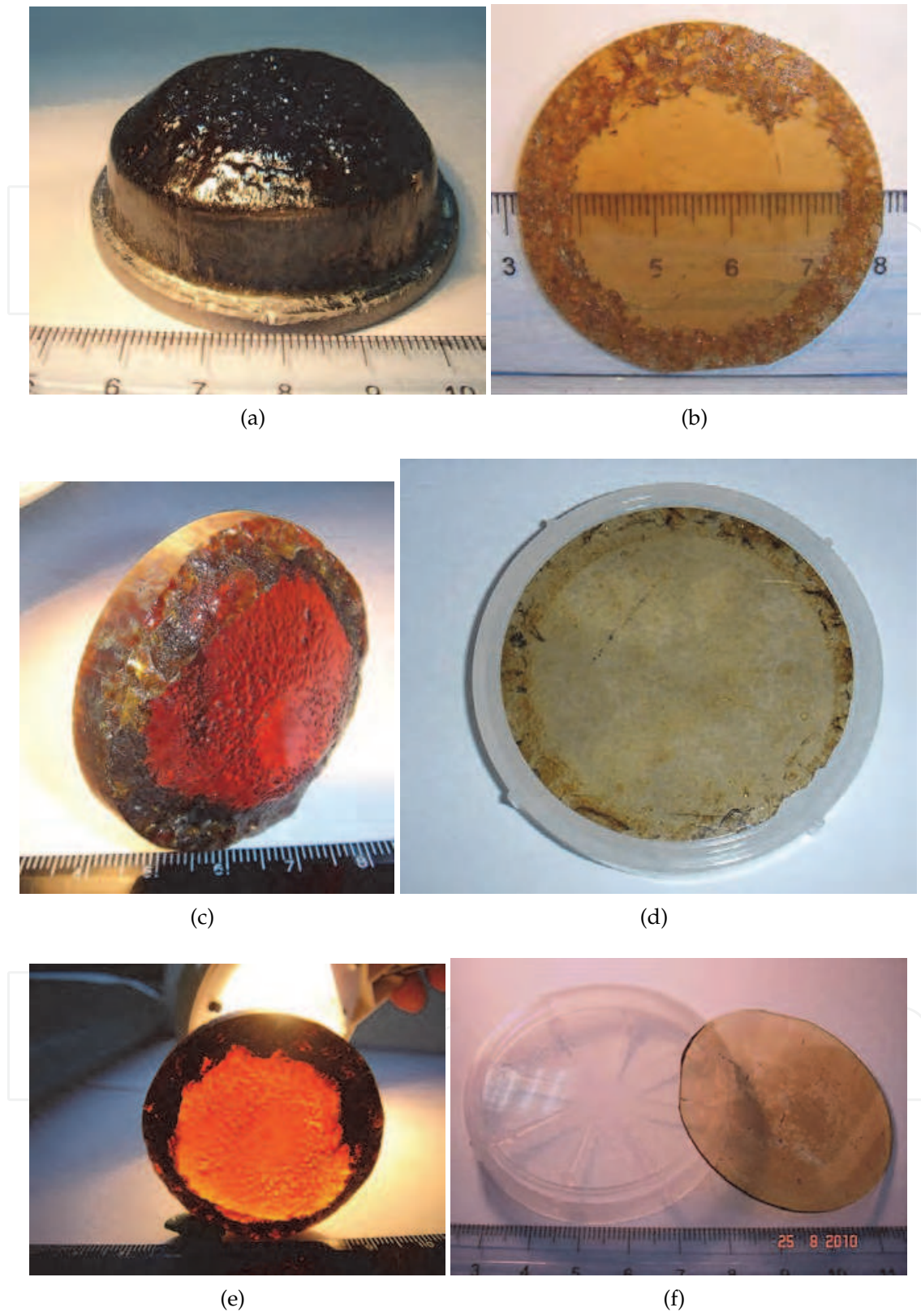
Fig. 12. Evolution of the quality of 2″ bulk AlN crystal (a, c, e) & corresponding substrate (b, d, f).

are rather high: about 5% Si and about 0.6 % C. However, the impurity concentration rapidly drops during the subsequent growth of the bulk AlN as could be seen from Fig. 13 where the variation of the concentration of aluminum, nitrogen, carbon, silicon and oxygen along the crystal thickness is shown.
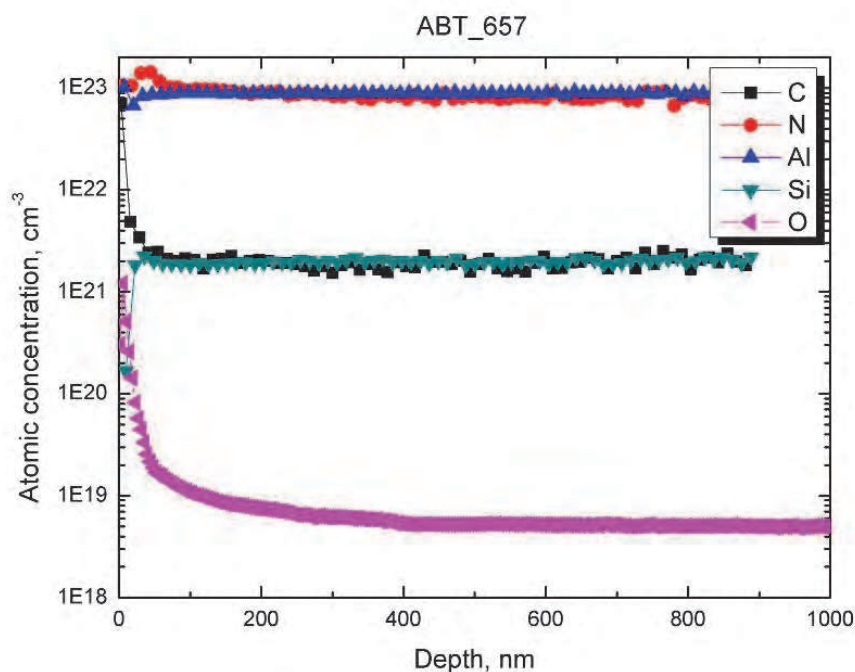

Fig. 13. Concentration of impurities along the crystal (Courtesy of V.V. Ber, Ioffe Physical Technical Institute, Russian Academy of Sciences).

X-ray diffractometry of the AlN substrates gives FWHMs of the rocking curves in ω-scan of about 2-5 arcmin. No impurities in concentrations higher than 100 ppm were found in the substrates. Typical data of X-ray analysis are presented in (Mokhov et al., 2005).

The resistivity of Si-doped AlN is generally lower than 10^5 Ohm·cm. These values are much lower than the reference resistivity of undoped semi-insulating AlN (10^{11}-10^{13} Ohm·cm). This result is attributed to the effect of the residual impurities (primarily Si) that still remain in the AlN bulk crystals grown on the SiC seeds. Repeated use of the initial AlN layer separated from the "primary" crystal (Chemekova et al., 2008) results in high purity material with the resistivity in the range of $3 \cdot 10^9$ - $3 \cdot 10^{11}$ Ohm · cm, which is rather close to the reference values.

Measurements of the transmittance spectrum of the substrates with thickness of 400 μm in the UV range have shown that most of the crystals have the average transmittance of 50-60% and demonstrate the sharp cut-off between 250nm and 320nm.

Selective etching in KOH/NaOH eutectic solution at 450°C reveals the presence of large grains with dislocation grain boundaries and individual dislocations with a low density (Fig. 14). The grain dimensions and the local dislocation densities can vastly differ.

The high crystallographic quality of the single crystal AlN substrate is confirmed by the Laue photo (Fig. 15, a) and the photo of the substrate in polarized light (Fig. 15, b).

The typical X-ray rocking curves of the 2in substrate at two different points are presented in Fig. 16.
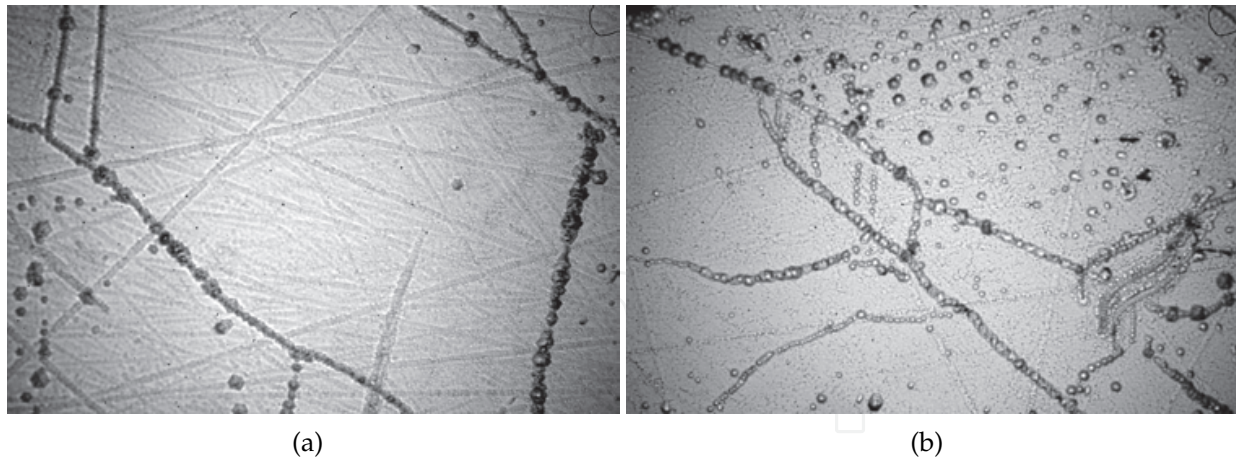
Fig. 14. Etched AlN surface (Courtesy of A. Polyakov, GIREDMET, Moscow).
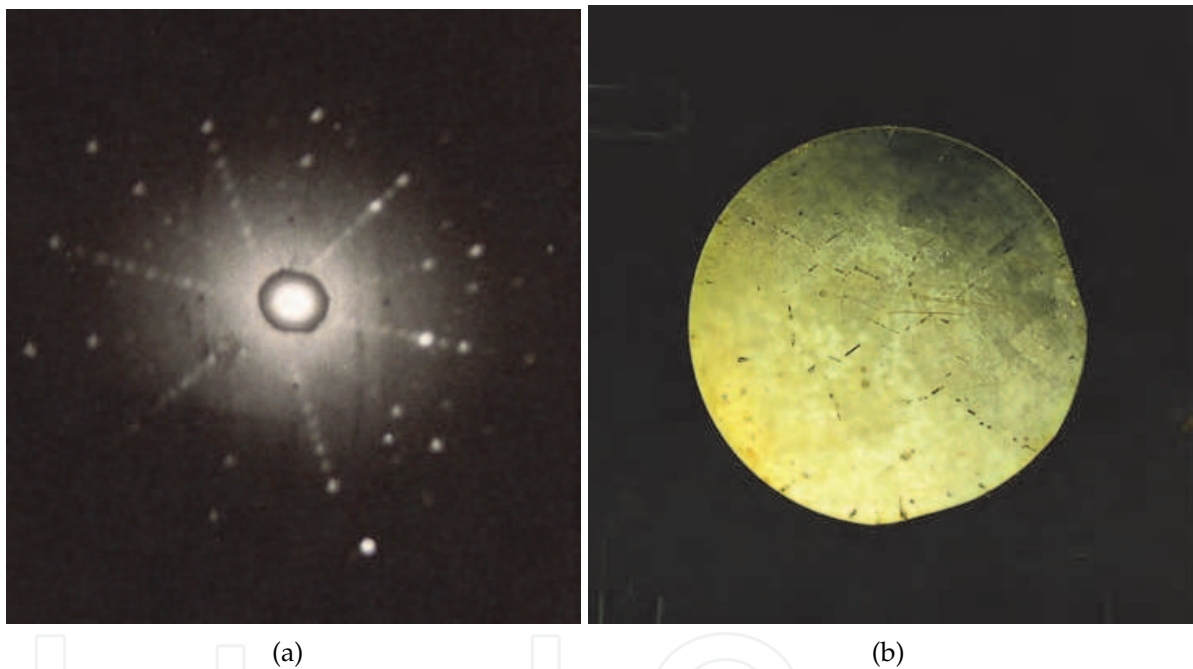

Fig. 15. Laue photo (a) and photo of 2in AlN substrate in polarized light (b).

6.1 Epitaxial layers

The best characteristic of the substrate is the quality of the grown epitaxial layers and the performance of the fabricated devices. The epitaxial structures deposited at bulk AlN have been studied using transmittance and reflectance optical microscopy, high-resolution XRD diffraction, cross-polarization and cathodoluminescence. The CL spectrum of the MOCVD grown 0.3 μm AlGaN layer (Fig. 17) has FWHM of about 10 nm that indicates layer-by-layer growth of the epitaxial film.

The morphology of 0.5μm AlN epitaxial layer grown on the 2in wafer could be assessed by the AFM images shown on Fig. 18. One could see large step bunches associated with the miscut of the wafer (1° for this wafer) off the (0001) axis. On the terraces between step bunches there are nice atomic steps.

(a)   (b)
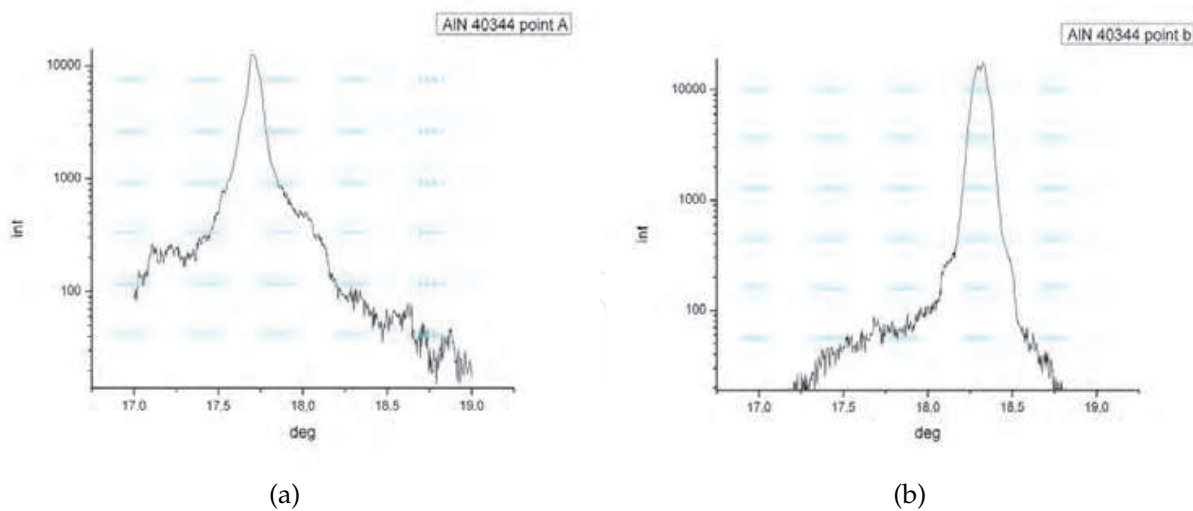
Fig. 16. X-ray rocking curves at different points of 2in substrate.
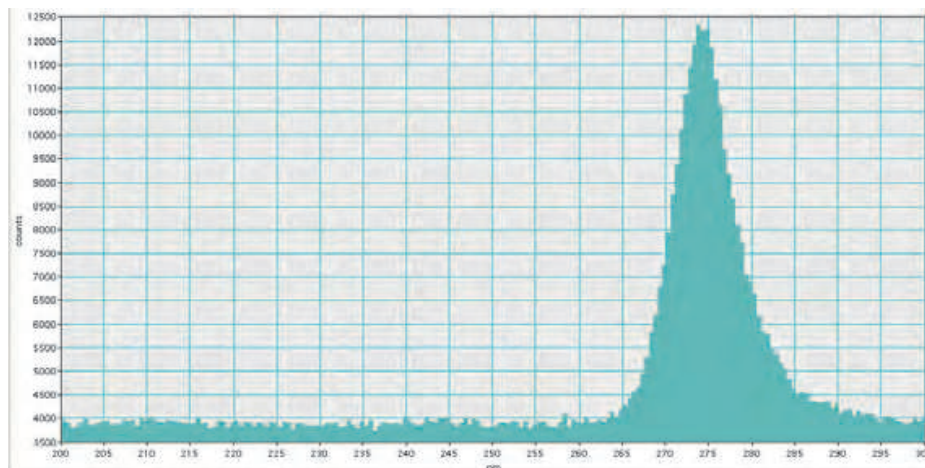
Fig. 17. CL spectrum of LED structure AlGaN/AlN (Courtesy of Prof. Asif Khan , University of South Carolina).

6.2 Light-emitting diodes

The emission of 5QW UV LED grown on bulk AlN substrate has a peak about 352 nm with FWHM 8 nm. The emission intensity was 4 times greater than that of the identical structure grown on sapphire (Fig. 19).

It should be stressed that the MOCVD growth procedure on the single crystal AlN substrate was not specially developed - the one optimized for the growth group III nitride epitaxial layers on sapphire was used.

UV LED emitting at 360 nm was grown by chloride VPE is shown in Fig. 20. This LED has a rather long lifetime: only a slight degradation is observed during long time operation (Fig. 21).

6.3 SAW applications

The surface acoustic wave velocity of the grown bulk AlN crystals measured at different frequencies and extrapolated to the zero frequency yields a value of about 5750 m/s.

(a) Image location on the substrate

(b) Center: 1 x 1 μm, Rms 0.97 nm

(c) Center: 3 x 3 μm, Rms 1.06 nm

(d) Center: 20 x 20 μm, Rms 1.02 nm

(e) Leading edge: 3 x 3 μm, Rms 1.61 nm

(f) Trailing edge: 3 x 3 μm, Rms 1.17 nm
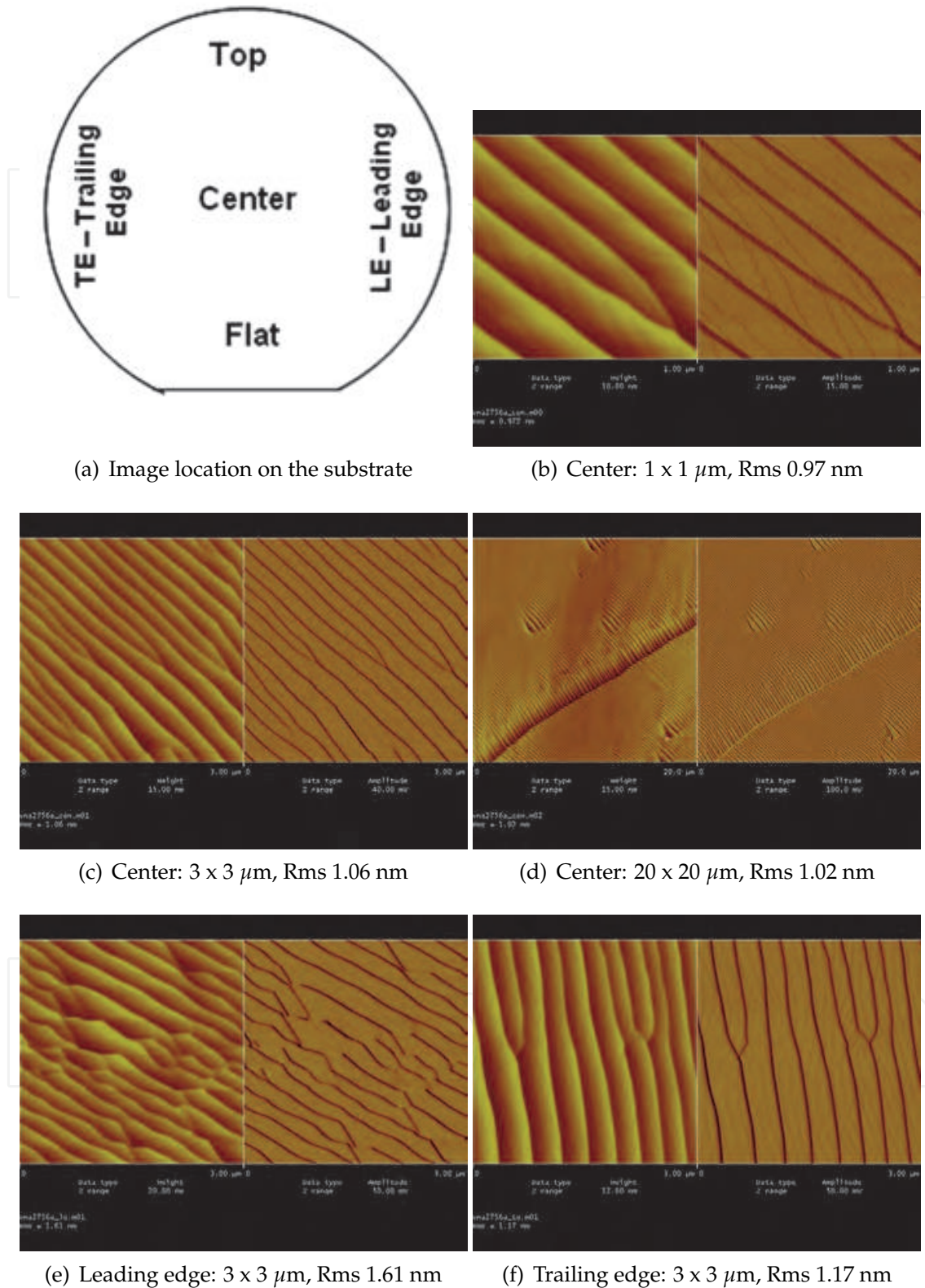
Fig. 18. AFM of AlN epitaxial layer on 2 inch bulk AlN substrate (Courtesy of A. Allerman, Sandia National Laboratory)
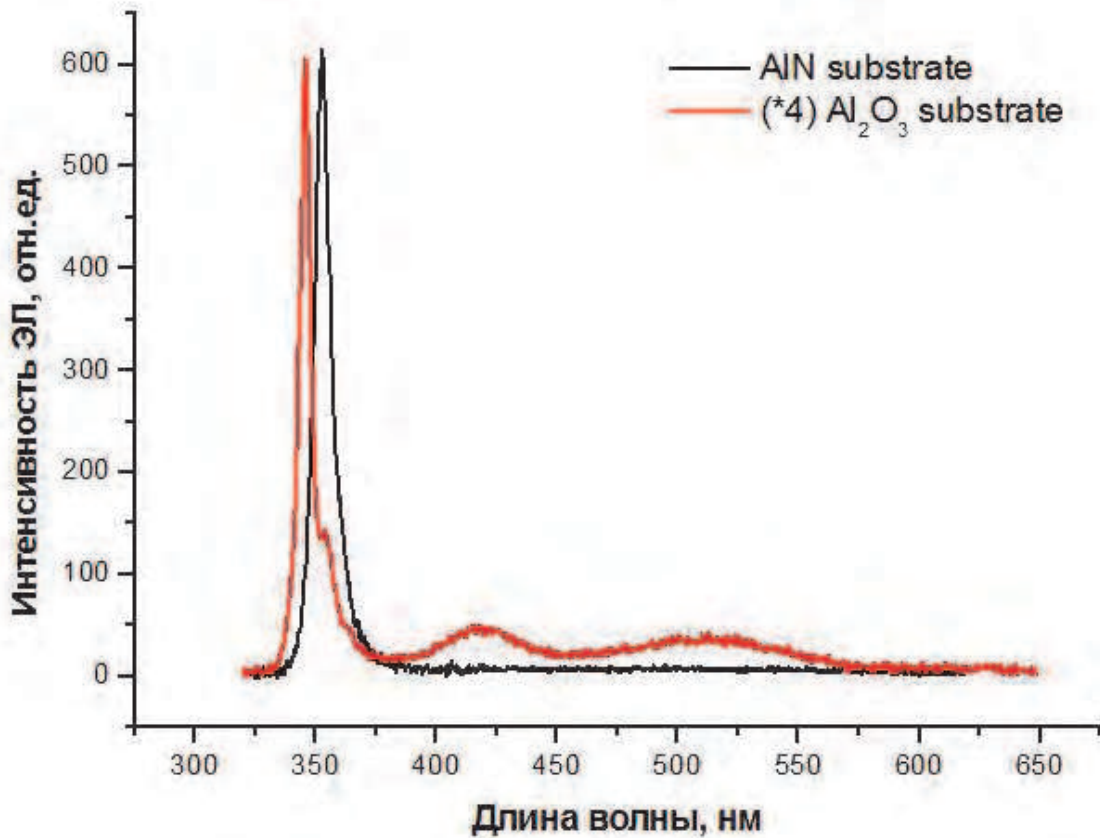
Fig. 19. EL intensity, that of UV LED on the sapphire substrate is increased fourfold (Courtesy of V.V. Lundin, Ioffe Physical Technical Institute, Russian Academy of Sciences).
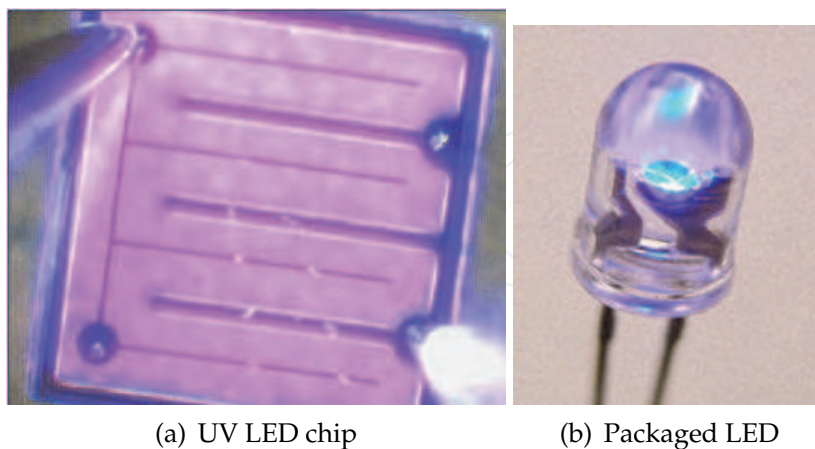
(a) UV LED chip   (b) Packaged LED

Fig. 20. 360 nm UV LED (Courtesy of The Fox Group, Inc.).

A simple regular electrode structure for SAW devices has been proposed in ref. (Biryukov et al., 2007). The structure consists of an interdigital transducer in the form of a ring placed on the Z cut of a hexagonal piezoelectric crystal (Fig. 22). Finite thickness electrodes produce the known slowing effect for a SAW in comparison with this SAW on a free surface. The closed
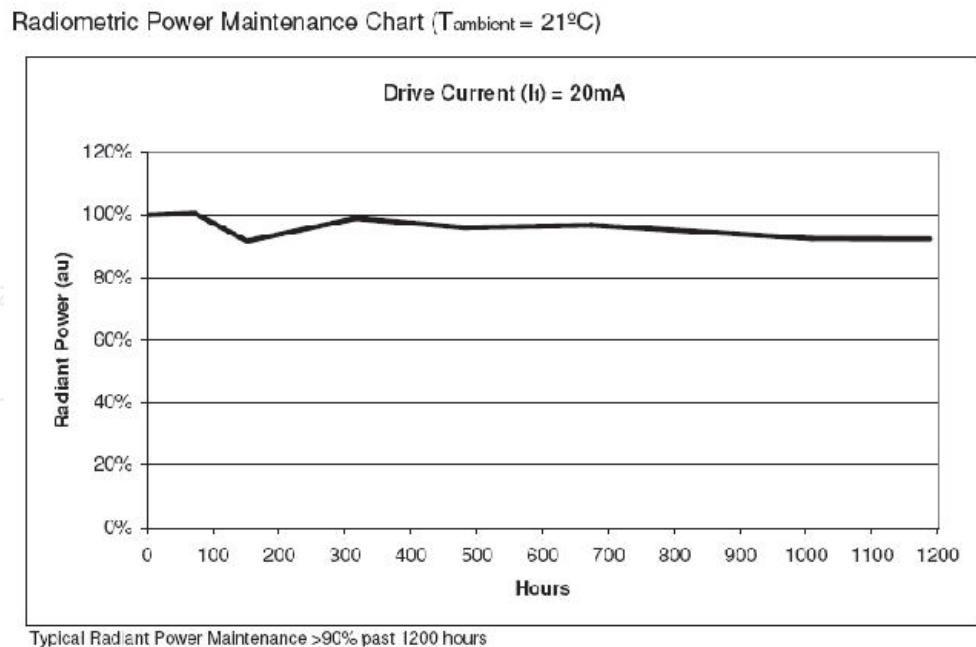
Fig. 21. Radiant power degradation (Courtesy of The Fox Group, Inc.).

slow electrode region with the *fast* surrounding region forms an open waveguide resonator structure with the acoustic field concentrated in the electrode region. If the radius of the structure - ring waveguide resonator (RWR) - is large enough for a given wavelength, an acceptable level of radiation losses can be reached. The electrical admittance of such resonator does not have sidelobes. Such device has been manufactored using a transparent pale brown
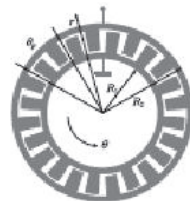
Fig. 22. Ring waveguide resonator on surface acoustic waves.

colored AlN single crystal wafer of 21 mm diameter and a thickness of 850 μm (Biryukov et al., 2009). Excitation of radial modes has been investigated. Experiments demonstrated the excellent device performance (high selectivity and a large Q-factor, estimated to be about 2700). The electrical admittance frequency dependence did not have sidelobes.

7. Conclusions

The technology of sublimation growth of AlN bulk crystals on the SiC seeds based on the successive use of crucibles made from different materials is described. Currently the technology provides stable growth of crystals up to 2" diameter and producing of single

crystal 2in AlN substrates. The superiority of such "good enough" AlN substrates for crystalline quality of the grown epitaxial layers and the device performance is demonstrated.

8. Acknowledgments

9. References

Abernathy, J. R. et al. (1979). Congruent (diffusionless) vapour transport, *J. Crystal Growth* 47: 145–154.

Adekore, B. T. et al. (2006). Ammonothermal synthesis of aluminum nitride crystals on group III-nitride templates, *J. Electron. Mater.* 35: 1104–1111.

AIAA (1998). Guide for the verification and validation of computational fluid dynamics simulations, AIAA G-077-1998.

Akasaki, I. & Amano, H. (2006). Breakthroughs in improving crystal quality of GaN and invention of the p-n junction blue-light-emitting diode, *Jap. J. Appl. Phys.* 454: 9001–9010.

Amano, H. et al. (2003). Group III nitride-based UV light emitting devices, *phys. stat. sol. (a)* 195: 491–495.

Ambacher, O. et al. (2003). Electronics and sensors based on pyroelectric AlGaN/GaN heterostructures. Part A: Polarization and pyroelectronics, *phys. stat. sol. (c)* 0: 1878–1907.

Angappan, S. et al. (2010). Aluminum nitride by microwave-assisted synthesis: Effect of added ammonia chloride, *Int. J. Self-Propag. High-Temp. Synthesis* 19: 214–220.

Aoki, M. et al. (2002). CrN single-crystal growth using Cr-Ga-Na ternary melt, *J. Crystal Growth* 246: 133–138.

Aoki, M. et al. (2002a). GaN single crystal growth using high-purity Na as a flux, *J. Crystal Growth* 242: 70–76.

Aoki, M. et al. (2000). Growth of GaN single crystals from a Na-Ga melt at 750° C and 5 MPa of N_2, *J. Crystal Growth* 218: 7–12.

Ashraf, H. et al. (2008). Thick GaN layers grown by HVPE: Influence of the templates, *J. Crystal Growth* 310: 3957–3963.

Avdeev, O. V. et al. (2010). Manufacturing of bulk AlN substrates, *in* P. Capper & P. Rudolph (eds), *Crystal Growth Technology: Semiconductors and Dielectrics*, Wiley-VCH Verlag GmbH & Co. KGaA, ISBN: 978-3-527-32593-1, pp. 121–136.

Avdeev, O. V. et al. (2011). Growth of bulk AlN crystals, *in* P. K. Bhattacharya et al. (eds), *Comprehensive Semiconductor Science and Technology*, Vol. 3, Elsevier Science Ltd, ISBN-10: 0444531432, ISBN-13: 9780444531438, pp. 282–301.

Avrutin, V. et al. (2010). Growth of bulk GaN and AlN: Progress and challenges, *Proceedings of the IEEE* 98: 1302 – 1315.

Bakhtizin, R. Z. et al. (2004). Scanning tunneling microscopy studies of III-nitride thin film heteroepitaxial growth, *Phys. Usp.* 47: 371–424.

Balkas, C. M. et al. (1997). Sublimation growth and characterization of bulk aluminum nitride single crystals, *J. Crystal. Growth* 179: 363–370.

Bao, H. Q. et al. (2009). The sublimation growth of AlN fibers: transformations in morphology & fiber direction, *Appl. Phys. A* 94: 173–177.

Beaumont, B. et al. (1998). Mg-enhanced lateral overgrowth of GaN on patterned GaN/sapphire substrate by selective metal organic vapor phase epitaxy, *MRS Internet J. Nitride Semicond. Res.* 3: 20.

Belousov, A. (2010). High pressure crystal growth, thermodynamics and physical properties of $Al_xGa_{1-x}N$ semiconductors, Dr. Sci. thesis, Eidgenössische Technische Hochschule, Zürich.

Belousov, A. et al. (2010). $Al_xGa_{1-x}N$ bulk crystal growth: Crystallographic properties and p-T phase diagram, *J. Crystal Growth* 312: 2585–2592.

Belousov, A. et al. (2009). Bulk single-crystal growth of ternary $Al_xGa_{1-x}N$ from solution in gallium under high pressure, *J. Crystal Growth* 311: 3971–3974.

Bennett, H. S. et al. (2004). Radio-frequency and analog/mixed-signal circuits and devices for wireless communications, *IEEE Circuits & Devices Magazine* pp. 38–51.

Bickermann, M. et al. (2010). UV transparent single-crystalline bulk AlN substrates, *phys. stat. sol. (c)* 7: 21–24.

Biryukov, S. V. et al. (2007). Ring waveguide resonator on surface acoustic waves, *Appl. Phys. Lett.* 90: 173503.

Biryukov, S. V. et al. (2009). Ring waveguide resonator on surface acoustic waves: First experiments, *J. Appl. Phys.* 106: 126103.

Bockowski, M. (2001). Growth and doping of GaN and AlN single crystals under high nitrogen pressure, *Cryst. Res. Technol.* 36: 771–787.

Bockowski, M. et al. (2001). Crystal growth of aluminum nitride under high pressure of nitrogen, *Mater. Sci. Semicond. Processing* 4: 543–548.

Bogdanov, M. V. et al. (2008). Coupled modeling of current spreading, thermal effects and light extraction in III-nitride light-emitting diodes, *Semicond. Sci. Technol* 23: 125023.

Bogdanov, M. V. et al. (2003). Advances in modeling of wide-bandgap bulk crystal growth, *Cryst. Res. Techn.* 38: 237–249.

Bogdanov, M. V. et al. (2001). Virtual reactor: a new tool for SiC bulk crystal growth study and optimization, *Mat. Sci. Forum* 353-356: 57–61.

Bogdanov, M. V. et al. (2004). Industrial challenges for numerical simulation of crystal growth, *Centr. Europ. J. Phys.* 2: 183.

Bondokov, R. T. et al. (2006). Defect content evaluation in single-crystal AlN wafers, *Mater. Res. Soc. Symp. Proc.* 892: FF30.

Bondokov, R. T. et al. (2007). Fabrication and characterization of 2-inch diameter AlN single-crystal wafers cut from bulk crystals, *Mater. Res. Soc. Symp. Proc.* 955: I03.

Bondokov, R. T. et al. (2008). Large-area AlN substrates for electronic applications: An industrial perspective, *J. Crystal Growth* 310: 4020–4026.

Brinkman, A. W. & Carles, J. (1998). The growth of crystals from the vapour, *Progr. Crystal Growth Character. Mater.* pp. 169–209.

Bulashevich, K. A. et al. (2007). Current spreading and thermal effects in blue LED dice, *Phys. Stat Solidi (c)* 4: 45–48.

Cai, D. et al. (2006). Thermal environment evolution and its impact on vapor deposition in large diameter AlN bulk growth. AIAA 2006-3825.

Cai, D. et al. (2010). Vapor growth of III nitrides, In: Springer Handbook of Crystal Growth, ISBN 978-3-540-74182-4, Eds. Dhanaraj et al., part F, 1243–1280.

Callahan, M. J. & Chen, Q. S. (2010). Hydrothermal and ammonothermal growth of ZnO and GaN, Ibid., part C, 655–689.

Cao, X. A. et al. (2004). Growth and characterization of blue and near-ultraviolet light-emitting diodes on bulk GaN, *Proc. SPIE* 5530: 48–53.

Cao, X. A. et al. (2007). Homoepitaxial growth and electrical characterization of GaN-based Schottky and light-emitting diodes, *J. Crystal Growth* 300: 382–386.

Cao, X. A. et al. (2004a). Electrical characteristics of InGaN/GaN light-emitting diodes grown on GaN and sapphire substrates, *Appl. Phys. Lett.* 85: 7–9.

Carter, C. B. & Norton, M. G. (2007). *Ceramic Materials, ISBN 978-0-387-46271-4*, Springer New York.

Cartwright, A. N. et al. (2006). Ultrafast carrier dynamics and recombination in green emitting InGaN MQW LED, *Mater. Res. Soc. Symp. Proc.* 916: DD04.

Chakraborty, A. et al. (2005). Demonstration of nonpolar *m*-plane InGaN/GaN light-emitting diodes on free-standing *m*-plane GaN substrates, *Jap. J. Appl. Phys.* 44: L173–L175.

Chemekova, T. Y. et al. (2008). Sublimation growth of 2 inch diameter bulk AlN crystals, *phys. stat. sol. (c)* 5: 1612–1614.

Chen, J. R. et al. (2007). Theoretical analysis of current crowding effect in Metal/AlGaN/GaN Schottky diodes and iIts reduction by using polysilicon in anode, *Chin. Phys. Lett.* 24: 2112–2114.

Chen, X. F. et al. (2008). Surface preparation of AlN substrates, *Cryst. Res. Technol.* 43: 651–655.

Cherns, D. (2000). The structure and optoelectronic properties of dislocations in GaN, *J. Phys.: Condens. Matter* 12: 10205–10212.

Cho, H. K. et al. (2000). Phase separation and stacking faults of $In_xGa_{1-x}N$ layers grown on thick GaN and sapphire substrate by metalorganic chemical vapor deposition, *J. Crystal Growth* 220: 197–203.

Choi, Y. S. et al. (2004). Effect of dislocations on the luminescence of GaN/InGaN multi-quantum-well light-emitting-diode layers, *Mater. Lett.* 58: 2614–2617.

Christen, J. et al. (2003). Optical micro-characterisation of group-III-nitrides: correleation of structural, electronic and optical properties, *phys. stat. sol. (c)* 0: 1795–1815.

Cleland, A. N. et al. (2001). Single-crystal aluminum nitride nanomechanical resonators, *Appl. Phys. Lett.* 79: 2070–2072.

Craford, M. G. (2005). LEDs for solid state lighting and other emerging applications: status, trends and challenges, *Proc. of SPIE* 5941: 594101.

Dalmau, R. F. (2005). Aluminum nitride biulk crystal growth in a resistively heated reactor, Ph. D. Thesis, North Carolina State University.

Dalmau, R. et al. (2005). AlN bulk crystals grown on SiC seeds, *J. Crystal Growth* 281: 68–74.

Dalmau, R. & Sitar, Z. (2005). Sublimation growth of AlN crystals, In: Encyclopedia of Materials: Science and Technology, Eds. K. H. J. Buschow et. al., pp. 1-9, Elsevier.

Dalmau, R. & Sitar, Z. (2010). AlN bulk crystal growth by physical vapor transport, In: Springer Handbook of Crystal Growth, ISBN 978-3-540-74182-4, Eds. Dhanaraj, G. et al., part D, 821–843.

Daryabeigi, K. (1999). Analysis and testing of high temperature fibrous insulation for reusable launch vehicles, AIAA 99-1044.

Davis, R. F. et al. (2001). Pendeo-epitaxial growth of thin films of gallium nitride and related materials and their characterization, *J. Crystal Growth* 225: 134–140.

Davis, R. F. et al. (2001a). Conventional and pendeo-epitaxial growth of GaN (0001) thin films on Si (111) substrates, *J. Crystal Growth* 231: 335–341.

Davis, R. F. et al. (2002). Gallium nitride materials - progress, status, and potential roadblocks, *Proc. IEEE* 90: 993–1005.

de Almeida, V. F. & Rojo, J. C. (2002). Simulation of transport phenomena in aluminum nitride single-crystal growth, Oak Ridge Nat. Lab., Tech. Rep. ORNL/TM-2002/64, 1–32.

Denis, A. et al. (2006). Gallium nitride bulk crystal growth processes; a review, *Mater. Sci. Eng.* R50: 167–194.

Detchprohm, T. et al. (2008). Green light emitting diodes on *a*-plane GaN bulk substrates, *Appl. Phys. Lett.* 92: 241109.

Detchprohm, T. et al. (2010). Wavelength-stable cyan and green light emitting diodes on nonpolar *m*-plane GaN bulk substrates, *Appl. Phys. Lett.* 96: 051101.

Dhanaraj, G. et al. (2003). Silicon carbide crystals - part I: Growth and characterization, *in* K. Byrappa & T. Ohashi (eds), *Crystal Growth Technology*, William Andrew Publishing, pp. 181–232.

Dinwiddie, R. B. et al. (1989). Thermal conductivity, heat capacity, and thermal diffusivity of selected commercial AlN substrates, *Int. J. Thermophys.* 10: 1075.

Dmitriev, V. & Usikov, A. (2006). Hydride vapor phase epitaxy of group III nitride materials, *in* Z. C. Feng (ed.), *III-nitride semiconductor materials*, ISBN-10: 1860946364, ISBN-13: 978-1860946363, World Scientific Publishing Company, pp. 1–40.

Dreger, L. H. et al. (1962). Sublimation and decomposition studies on boron nitride and aluminum nitride, *J. Phys. Chem.* 66: 1556–1559.

Dryburgh, P. M. (1992). The estimation of maximum growth rate for aluminium nitride crystals grown by direct sublimation, *J. Crystal Growth* 125: 65–68.

Du, L. & Edgar, J. H. (2010). Thermodynamic analysis and purification for the source materials in sublimation crystal growth of aluminum nitride, *Mater. Res. Soc. Symp.* 1202: I05–08.

Du, L. et al. (2010). Sublimation growth of titanium nitride crystals, *J. Mater. Sci.: Mater. Electron.* 21: 78–87.

Du, X. Z. et al. (2010). UV light-emitting diodes at 340 nm fabricated on a bulk GaN substrate, *Chin. Phys. Lett.* 27: 088105.

Dupret, F. et al. (1990). Global modeling of heat transfer in crystal growth furnaces, *Int. J. Heat Mass Transfer* 33: 1849–1871.

Edgar, J. H. et al. (2008). Native oxides and hydroxides and their implications for bulk AlN crystal growth, *J. Crystal Growth* 310: 4002–4006.

Edgar, J. H. et al. (eds) (1999). *Properties, processing and applications of GaN and related semiconductors*, INSPEC, the IEE, London.

Egorov, Y. & Zhmakin, A. (1998). Numerical simulation of low-Mach number gas mixture flows with heat and mass transfer using unstructured grid, *Comput. Mat. Sci.* 11: 204–220.

Ehrentraut, D. & Fukuda, T. (2008). Bulk zinc oxide and gallium nitride crystals by solvothermal techniques, *in* Y. Fujikawa et al. (eds), *Frontiers in Materials Research*, Springer, pp. 111–120.

Ehrentraut, D. & Fukuda, T. (2010). The ammonothermal crystal growth of gallium nitride - a technique on the up rise, *Proceedings of the IEEE* 98: 1316 – 1323.

Ehrentraut, D. & Kagamitanii, Y. (2010). Acidic ammonothermal growth technology for GaN, *in* Hull, R. et al. (eds), *Technology of Gallium Nitride Crystal Growth, , ISBN 978-3-642-04830-2*, Vol. 133 of *Springer Series in Materials Science*, Springer Berlin Heidelberg, pp. 183–203.

Ehrentraut, D. et al. (2006). Solvothermal growth of ZnO, *Prog. Cryst. Growth Charact. Mater.* 52: 280–335.

Eisenberg, H. R. & Kandel, D. (2002). Origin and properties of the wetting layer and early evolution of epitaxially strained thin films, *Phys. Rev. B* 66: 155429.

Epelbaum, B. et al. (2002). Sublimation growth of bulk AlN crystals: materials compatibility and crystal quality, *Mater. Sci. Forum* 433–436: 983–986.

Epelbaum, B. et al. (2001). Seeded PVT Growth of Aluminum Nitride on Silicon Carbide, *Mat. Sci. Form* 389-393: 1445–1448.

Epelbaum, B. M. et al. (2004). Growth of bulk AlN crystals for SAW devices, Proc. Second Int. Symp.on Acoustic Wave Devices for Future Mobile Comm. Systems, Chiba, March 2004, 157–162.

Ern, A. & Guermond, J. L. (2004). Accurate numerical simulation of radiative heat transfer with application to crystal growth, *Int. J. Numer. Meth. Engineer.* 61: 559–583.

Evstratov, I. Y. et al. (2006). Current crowding effects on blue LED operation, *Phys. stat. sol.(c)* 3: 1645 – 1648.

Fan, Z. Y. et al. (2006). AlGaN/GaN/AlN quantum-well field-effect transistors with highly resistive AlN epilayers, *Appl. Phys. Lett.* 88: 073513.

Fan, Z. Y. & Newman, N. (2001). Experimental determination of the rates of decomposition and cation desorption from AlN surfaces, *Mat. Sci. Eng. B* 87: 244–248.

Fara, A. et al. (1999). Theoretical evidence for the semi-insulating character of AlN, *Appl. Phys. Lett.* 85: 2001–2003.

Fini, P. et al. (1998). The effect of growth environment on the morphological and extended defect evolution in GaN grown by metalorganic chemical vapor deposition, *Jap. J. Appl. Phys.* 37: 4460–4466.

Frank, F. C. & van der Merwe, J. (1949). One dimensional dislocations. II. Misfit monolayers and oriented overgrowth, *Proc. Roy. Soc.(London) A* 198: 216–225.

Franko, A. & Shanafield, D. J. (2004). The thermal conductivity of polycrystalline aluminum nitride (AlN) ceramics, *Ceramica* 50: 247–253.

Frayssinet, E. et al. (2001). Evidence of free carrier concentration gradient along the c-axis for undoped GaN single crystals, *J. Crystal Growth* 230: 442–447.

Freitas, J. A. (2005). Bulk and homoepitaxial films of III-V nitride semiconductors: Optical studies, *J. Ceramic Process. Res.* 6: 209–217.

Freitas, J. A. (2010). Properties of the state of the art of bulk III-V nitride substrates and homoepitaxial layers, *J. Phys. D: Appl. Phys.* 43: 073301.

Freund, L. (1995). Evolution of waviness of the surface of a strained elastic solid due to stress-driven diffusion, *Int. J. Solid Structures* 32: 911–923.

Fritze, H. (2011). High-temperature piezoelectric crystals and devices, *J. Electroceram.* 26: 122–161.

Fukuda, T. & Ehrebtraut, D. (2007). Prospects for the ammonothermal growth of large GaN crystals, *J. Crystal Growth* 305: 304–310.

Fukuyama, H. et al. (2006). Single crystalline aluminum nitride films fabricated by nitriding α-SiO$_2$, *Appl. Phys. Lett.* 100: 024905.

Gaska, R. et al. (2002). Deep-ultraviolet emission of AlGaN/AlN quantum wells on bulk AlN, *Appl. Phys. Lett.* 81: 4658–4660.

Gautier, S. et al. (2008). AlGaN/AlN multiple quantum wells grown by MOVPE on AlN templates using nitrogen as a carrier gas, *J. Crystal Growth* 310: 4927–4931.

Gilmer, G. H. et al. (1998). Thin film deposition: fundamentals and modeling, *Comput. Mater. Sci.* 12: 354–380.

Golan, Y. et al. (1998). Morphology and microstructural evolution in the early stages of hydride vapor phase epitaxy of GaN on sapphire, *Appl. Phys. Lett.* 73: 3090–3092.

Grandusky, J. J. et al. (2010). Properties of mid-ultraviolet light emitting diodes fabricated from pseudomorphic layers on bulk aluminum nitride substrates, *Appl. Phys. Express* 3: 072103.

Grandusky, J. J. et al. (2009). Pseudomorphic growth of thick n-type $Al_xGa_{1x}N$ layers on low-defect-density bulk AlN substrates for UV LED applications, *J. Crystal Growth* 311: 2864–2866.

Gromov, A. A. et al. (2005). Nitride formation during combustion of ultrafine aluminum powder in air. I. Effect of additives, *Combustion, Explosion and Shock Waves* 41: 303–314.

Grzegorczyk, A. P. et al. (2005). Influence of sapphire annealing in trimethylgallium atmosphere on GaN epitaxy by MOCVD, *J. Crystal Growth* 283: 72–80.

Grzegory, I. (2001). High pressure growth of bulk GaN from solutions in gallium, *J. Phys.: Condens Matter* 13: 6875–6892.

Grzegory, I. et al. (2002). Mechanisms of crystallization of bulk GaN from the solution under high N_2 pressure, *J. Crystal Growth* 246: 177–186.

Han, Q. et al., Q. H. (2008). Polarity analysis of self-seeded aluminum nitride crystals grown by sublimation, *J. Electron. Mater.* 37: 1058–1063.

Hartmann, C. et al. (2008). Homoepitaxial seeding and growth of bulk AlN by sublimation, *J. Crystal Growth* 310: 930–934.

Hashimoto, S. et al. (2010). Epitaxial layers of AlGaN channel HEMTs on AlN substrates, *SEI Techn. Rev.* 71: 83–87.

Helava, H. et al. (2007). Growth of bulk aluminum nitride crystals, *phys. stat. sol. (c)* 4: 2281–2284.

Hemmingsson, C. et al. (2010). Growth of III-nitrides with halide vapor phase epitaxy (HVPE), In: Springer Handbook of Crystal Growth, ISBN 978-3-540-74182-4, Eds. Dhanaraj, G. et al., part D, 869–896.

Herro, Z. D. et al. (2006). Growth of large AlN single crystals along the [0001] direction, *Mater. Res. Soc. Symp. Proc.* 892: FF21.

Heying, B. et al. (1999). Dislocation mediated surface morphology of GaN, *J. Appl. Phys.* 85: 6470–6476.

Hirano, T. et al. (2009). Synthesis of GaN crystal by the reaction of Ga with Li_3N in NH_3 atmosphere, *J. Crystal growth* 311: 3040-3043.

Hovakimian, L. B. (2009). Strong-coupling theory of mobility collapse in GaN layers, *Appl. Phys. A* 96: 255–257.

Hu, X. et al. (2003). AlGaN/GaN heterostructure field-effect transistors on single-crystal bulk AlN, *Appl. Phys. Lett.* 82: 1299–1301.

Hull, R. et al. (2002). Interaction between surface morphology and misfit dislocations as strain relaxation modes in lattice-mismatched heteroepitaxy, *J. Phys.: Condens. Matter* 14: 12829–12841.

Hull, R. & Stach, E. A. (1996). Equilibrium and metastable strained layer semiconductor structures, *Current Opinion in Solid State & Mater. Sci.* 1: 21–28.

Hung, A. et al. (2004). An *ab initio* study of structural properties and single vacancy defects in wurtzite AlN, *J. Chem. Phys.* 120: 4890–4896.

I-hsiu, H. & Stringfellow, G. B. (1996). Solid phase immiscibility in GaInN, *Appl. Phys. Lett.* 69: 2701–2703.

Ilyin, I. V. et al. (2010). Deep-level defects in AlN single crystals: EPR studies, *Mater. Sci. Forum* 645–648: 1195–1198.

Iwahashi, T. et al. (2003). Effects of ammonia gas on threshold pressure and seed growth for bulk GaN single crystals by Na flux method, *J. Crystal Growth* 253: 1–5.

Iwasaki, F. & Iwasaki, H. (2002). Historical review of quartz crystal growth, *J. Crystal Growth* 237-239: 820.

Jain, S. C. et al. (1997). Misfit strain and misfit dislocations in lattice mismatched epitaxial layers and other systems, *Phil. Mag. A* 75: 1461–1515.

Jain, S. C. & Hayes, W. (1991). Structure, properties and applications of Ge_xSi_{1x} strained layers and superlattices, *Semicond. Sci. Technol.* 6: 547–576.

Jain, S. C. et al. (2000). III-nitrides: growth, characterization, and properties, *J. Appl. Phys.* 87: 965–1006.

Kallinger, B. et al. (2008). Vapor growth of GaN using GaN powder sources and thermographic investigations of the evepoarting behaviour of the source material, *Cryst. Res. Techn.* 43: 14–21.

Karpov, D. et al. (2001a). Mass transport and powder source evolution in sublimation growth of SiC bulk crystals, *Mat. Sci. Forum.* 353-356: 37–40.

Karpov, S. Y. (1998). Suppression of phase separation in InGaN due to elastic strain, *MRS Internet J. Nitride Semicond. Res.* 3: 16.

Karpov, S. Y. (2009). Bandgap engineering of III-nitride devices on low-defect substrates, *in* Z. C. Feng (ed.), *III-Nitride Devices and Nanoengineering*, Imperial College Press, London, pp. 367–398.

Karpov, S. Y. et al. (2001). Effect of reactive ambient on AlN sublimation growth, *phys. stat. sol. (a)* 188: 763–767.

Karpov, S. Y. et al. (2003). Role of oxygen in AlN sublimation growth, *phys. stat. sol. (c)* 0: 1989–1992.

Karpov, S. Y. et al. (1999). Sublimation growth of AlN in vacuum and in a gas atmosphere, *phys. stat. sol. (a)* 176: 435–438.

Kasap, S. & Capper, P. (eds) (2006). *Springer Handbook of Electronic and Photonic Materials, ISBN 978-0-387-29185-7*, Springer.

Kawahara, M. et al. (2005). A systematic study on the growth of GaN single crystals using Na-based flux method, *J. Ceramic Process. Res.* 6: 146–152.

Kazan, M. et al. (2006). What causes rough surface in AlN crystals?, *J. Crystal Growth* 290: 44–49.

Kazan, M. et al. (2006a). Phonon dynamics in AlN lattice contaminated by oxygen, *Diamond Rel. Mater.* 15: 1525–1534.

Ketchum, D. R. & Kolis, J. W. (2001). Crystal growth of gallium nitride in supercritical ammonia, *J. Crystal Growth* 222: 431–434.

Kirchner, C. et al. (1999). Homoepitaxial growth of GaN by metal-organic vapor phase epitaxy: A benchmark for GaN technology, *Appl. Phys. Lett.* 75: 1098–1100.

Kitanin, E. et al. (1998). Heat transfer through source powder in sublimation growth of SiC crystal, *Mater. Sci. Eng.* B55: 174–183.

Klapper, H. (2010). Generation and propagation of defects during crystal growth, *in* G. Dhanaraj et al.(eds), *Springer Handbook of Crystal Growth, ISBN 978-3-540-74182-4*: 93–116.

Kochuguev, S. K. et al. (2001). Solution of crystal growth problems using adaptive unstrucured grids, *in* M. Baines (ed.), *Numerical Methods for Fluid Dynamics VII*, ISBN-10: 095249292X, ISBN-13: 978-0952492924, Oxford University Press, pp. 363–369.

Korcak, S. et al. (2007). Structural and optical properties of an $In_xGa_{1-x}N/GaN$ nanostructure, *Surf. Sci.* 601: 3892–3897.

Krukowski, S. (1997). Thermodynamics and high-pressure growth of (Al, Ga, In)N single crystals, *Diamond and Related Materials* 6: 1515–1523.

Kukushkin, S. A. et al. (2008). Substrates for epitaxy of gallium nitride; new materials and techniques, *Rev. Adv. Mater. Sci* 17: 1–32.

Kumagai, Y. et al. (2008). Self-separation of a thick AlN layer from a sapphire substrate via interfacial voids formed by the decomposition of sapphire, *Appl. Phys. Express* 1: 045003.

Kuwano, N. et al. (2004). Formation and annihilation of threading dislocations associated with stress in hetero-structure of GaN and AlGaN, *IPAP Conf. Series* 4: 21–24.

Lee, H. et al. (2004). Preparation of freestanding GaN and GaN template by hybride vapor phase epitaxy, *IPAP Conf. Series* 4: 25–27.

Lee, R. G. (2007). Transmission electron microscopy and thermal residual stress analysis of AlN crystal. MS thesis, Texas Tech UniverSity.

Lim, Y. S. et al. (2000). Strain-induced diffusion in a strained $Si_{1-x}Ge_x/Si$ heterostructure, *Appl. Phys. Lett.* 77: 4157–4159.

Limb, J. B. (2007). Design, fabrication and characterization of III-nitride pn junction devices, PhD thesis, Georgia Institute of Technology.

Lin, G. Q. et al. (2008). Influence of AlN buffer thickness on GaN grown on Si(111) by gas source molecular beam epitaxy with ammonia, *Chin. Phys. Lett.* 25: 4097–4100.

Liu, W. & Balandin, A. A. (2005). Thermal conduction in $Al_xGa_{1-x}N$ alloys and thin films, *J. Appl. Phys.* 97: 073710.

Liu, Y. S. (2009). An overview of the development of major light sources; from light bulbs to solid state lighting, *in* Z. C. Feng (ed.), *III-Nitride Devices and Nanoengineering*, Imperial College Press, London, pp. 1–20.

Louarn, A. L. et al., Vézian, S., Semond, F. & Massies, J. (2009). AlN buffer layer growth for GaN epitaxy on (111) Si: Al or N first?, *J. Crystal Growth* 311: 3278–3284.

Lu, P. (2006). Sublimation growth of AlN bulk crystals and high-speed CVD growth of SiC epilayers, and their characterization, Ph. D. thesis, Kansas State Univ.

Lu, P. et al. (2008). Seeded growth of AlN on SiC substrates and defect characterization, *J. Crystal Growth* 310: 2464–2470.

Luft, J. et al. (1999). Microbatch macromolecular crystallization on a thermal gradient, *J. Crystal Growth* 196: 447–449.

Luo, B. et al. (2002). High breakdown M-I-M structures on bulk AlN, *Solid-State Electron.* 46: 573–576.

Majewski, J. A. & Vogl, P. (1998). Polarization and band offsets of stacking faults in AlN and GaN, *MRS Internet J. Nitride Semicond. Res.* 3: 21.

Makarov, Y. & Zhmakin, A. (1989). On flow regimes in VPE reactors, *J. Crystal Growth* 94: 537–551.

Matsuoka, T. (2005). Progress in nitride semiconductors from GaN to InN - MOVPE growth and characteristics, *Superlatt. and Micristruct.* 37: 19–32.

Matthews, J. W. & Blakeslee, A. E. (1974). Defects in epitaxial multilayers.I. Misfit dislocations, *J. Crystal Growth* 27: 118–125.

McAleese, C. et al. (2006). Electric fields in AlGaN/GaN quantum well structures, *phys. stat. sol. (b)* 243: 1551–1559.

Medraj, M. et al. (2005). Understanding of AlN sintering through computational thermodynamics combined with experimental investigation, *J. Mat. Process. Technol.* 161: 415–422.

Meissner, E. et al. (2004). Growth of GaN crystals and epilayers from solutions at ambient pressure, *IPAP Conf. Series* 4: 46–49.

Miskys, C. R. et al. (2003). Freestanding GaN-substrates and devices, *phys. stat. sol. (c)* 0: 1627–1650.

Miyajima, T. et al. (2001). GaN-based blue laser diodes, *J. Phys.: Condens. Matter* 13: 7099–7114.

Miyanaga, M. et al. (2006). Single crystal growth of AlN by sublimation method, *SEI Techn. Rev.* 63: 22–25.

Miyoshi, T. et al. (2009). 510–515 nm InGaN-based green laser diodes on *c*-plane GaN substrates, *Appl. Phys. Express.* 2: 062201.

Mokhov, E. N. et al. (2005). Sublimation growth of AlN bulk crystals in Ta crucibles, *J. Crystal Growth* 281: 93–100.

Mokhov, E. N. et al. (2002). Growth of AlN bulk crystals by sublimation sandwich method, *Mat. Sci. Forum* 433-436: 979–982.

Moran, B. et al. (2000). Growth and characterization of graded AlGaN conducting buffer layers on n^+ SiC substrates, *J. Crystal Growth* pp. 301–304.

Morkoc, H. (1998). *Wide Band Gap Nitrides and Devices*, Springer, Berlin.

Mukai, T. et al. (2001). Nitride light-emitting diodes, *J. Phys.: Condens. Matter* 13: 7089–7098.

Müller, E. et al. (2006). Electrical activity of dislocations in epitaxial ZnO- and GaN-layers analyzed by holography in a transmission electron microscope, *Mat. Sci. in Semicond. Processing* 9: 127–131.

Mymrin, V. F. et al. (2005). Bandgap engineering of electronic and optoelectronic devices on native AlN and GaN substrates: a modelling insight, *J. Crystal Growth* 281: 115–124.

Nakamura, S. et al. (2000). *The Blue Laser Diode (2nd ed.)*, ISBN-10: 3642085792, ISBN-13: 978-3642085796, Springer, N. Y.

Nam, O. H. et aL. (1997). Lateral epitaxy of low defect density GaN layers via organometallic vapor phase epitaxy, *Appl. Phys. Lett.* 71: 2638–2640.

Nam, O. H. et al. (1998). Lateral epitaxial overgrowth of GaN films on SiO_2 areas via metal-organic vapor phase epitaxy, *J. Electron. Mater.* 27: 233–237.

Nanjo, T. et al. (2008). Remarkable breakdown voltage enhancement in AlGaN channel high electron mobility transistors, *Appl. Phys. Lett.* 92: 263502.

Nause, J. & Nemeth, B. (2005). Pressurized melt growth of ZnO boules, *Semicond. Sci. Technol.* 20: S45–S48.

Nikolaev, A. et al. (2000). AlN wafers fabricated by hydride vapor phase epitaxy, *MRS Internet J. Nitride Semicond. Res.* 5S1: W6.5.

Nishida, T. et al. (2004a). AlGaN-based ultraviolet light-emitting diodes grown on bulk AlN substrates, *Appl. Phys. Lett.* 84: 1002–1003.

Nishida, T. et al. (2004b). High current injection to a UV-LED grown on bulk AlN substrates, *MRS Proc.* 798: Y1.3.

Nishino, K. et al. (2002). Bulk GaN by direct synthesis method, *J. Crystal Growth* 237-239: 922–925.

Nord, J. et al. (2003). Modelling of compound semiconductors: analytical bond-order potential for gallium, nitrogen and gallium nitride, *J. Phys.: Condens Matter* 15: 5649.

Northrup, J. E. (2005). Shallow electronic states induced by prismatic stacking faults in AlN and GaN, *Appl. Phys. Lett.* 86: 071901.

Noveski, V. et al. (2004a). Growth of AlN crystals on AlN/SiC seeds by AlN powder sublimation in nitrogen atmosphere, *MRS Internet J. Nitride Semicond. Res.* 9: 2.

Noveski, V. et al. (2004b). Mass transfer in AlN crystal growth at high temperatures, *J. Crystal Growth* 266: 369–378.

Oden, J. T. (2002). The promise of Computational Engineering and Science: will it be kept?, *IACM Express* (12): 12–15.

Oh, T. S. et al. (2009). Epitaxial growth of improved GaN epilayer on sapphire substrate with platinum nanocluster, *J. Crystal Growth* 311: 2655–2658.

Ohtani, N. et al. (2007). Crystal growth, *in* K. Nakahashi et al., *Wide Bandgap Semiconductors. Fundamental Properties and Modern Photonic and Electronic Devices. ISBN 10-3-540-47234-7*, Springer Berlin Heidelberg New York, pp. 329–446.

Okamoto, K. et al. (2009). Epitaxial growth of GaN on single-crystal Mo substrates using HfN buffer layers, *J. Crystal Growth* 311: 1311–1315.

Onda, M. et al. & Sasaki, T. (2002). Influence of pressure control on the growth of bulk GaN single crystal using a Na flux, *J. Crystal Growth* 237-239: 2112–2115.

Orton, J. W. & Foxon, C. T. (1998). Group III nitride semiconductors for short wavelength light-emitting devices, *Rep. Prog. Phys.* 61: 1–75.

Ougazzaden, A. et al. (2008). Growth of GaN by metalorganic vapor phase epitaxy on ZnO-buffered c-sapphire substrates, *J. Crystal Growth* 310: 944–947.

Paskova, T. et al. (2010). GaN substrates for III-nitride devices, *Proc. IEEE* 98: 1324–1338.

Paskova, T. et al. (2009). Polar and non-polar HVPE GaN substrates: Impact of doping on the structural, electrical and optical characteristics, *phys. stat. sol.* pp. S344–S347.

Paskova, T. et al. (2004). Growth, separation and properties of HVPE grown GaN films using different nucleation schemes, *IPAP Conf. Series* 4: 14–20.

Pearton, S. J. et al. (2000). Fabrication and performance of GaN electronic devices, *Mater. Sci. Eng.* 30: 55–212.

Pecz, B. et al. (2008). Composite substrates for GaN growth, *in* A. G. Cullis & P. A. Midgley (eds), *Microscopy of Semiconducting Materials, ISBN 978-1-4020-8614-4, 2007*, Springer Netherlands, pp. 53–56.

Perlin, P. et al. (2005). Properties of InGaN blue laser diodes grown on bulk GaN substrates, *J. Crystal Growth* 281: 107–114.

Pinnington, T. et al. (2008). InGaN/GaN multi-quantum well and LED growth on wafer-bonded sapphire-on-polycrystalline AlN substrates by metalloorganic chemical vapor deposition, *J. Crystal Growth* 310: 2514–2519.

Porowski, S. & Grzegory, I. (1997). Thermodynamical properties of III-V nitrides and crystal growth of GaN at high N_2 pressure, *J. Crystal Growth* 178: 174–188.

Potin, V. et al. (1998). Extended defects in nitride semiconductors, *J. Electron. Mater.* 27: 266–275.

Purdy, A. P. et al. (2003). Synthesis of GaN by high-pressure ammonolysis of gallium triiodide, *J. Crystal Growth* 252: 136–143.

Radwan, M. & Miyamoto, Y. (2006). Self-propagating high-temperature synthesis of AlN nanostructures and their sintering properties, *Trans. of JWRI* 35: 43–46.

Raghothamachar, B. et al. (2006). Characterization of bulk grown GaN and AlN single crystal materials, *J. Crystal Growth* 287: 349–353.

Raghothamachar, B. et al. (2003). X-ray characterization of bulk AlN single crystals grown by the sublimation technique, *J. Crystal Growth* 250: 244–250.

Ram-Mohana, L. R. et al. (2006). Wavefunction engineering of layered wurtzite semiconductors grown along arbitrary crystallographic directions, *Superlattices and Microstructures* 39: 455–477.

Ren, Z. et al. (2007). Heteroepitaxy of AlGaN on bulk AlN substrates for deep ultraviolet light emitting diodes, *Appl. Phys. Lett.* 91: 051116.

Ren, Z. et al. (2007a). AlGaN deep ultraviolet LEDs on bulk AlN substrates, *phys. stat. sol. (c)* 4: 2482–2485.

Rojas, T. C. et al. & García, R. (1998). Relaxation mechanism of InGaAs single and graded layers grown on (111)B GaAs, *Thin Solid Films* 317: 270–273.

Rojo, C. J. et al. (2006). Physical vapor transport crystal growth of ZnO, *Proc. of SPIE* 6122: 61220Q1.

Rojo, J. C. et al. (2001). Single-crystal aluminum nitride substrate preparation from bulk crystals, *Mat. Res. Soc. Symp. Proc.* 680: E2.1.

Rojo, J. C. et al. (2002). Progress in the preparation of aluminum nitride substrates from bulk crystals *Mat. Res. Soc. Symp. Proc.* 722: K1.1.1.

Roycroft, B. et al. (2004). Origin of power fluctuations in GaN resonant-cavity light-emitting diodes, *Opt. Express* 12: 736–741.

Russel, P. (2006). SiC, sapphire and GaN materials status in Opto and RF business, Proc. CS MANTECH Conf., Vancouver, 231-232.

Satoh, I. et al. (2010). Development of aluminum nitride single-crystal substrates, *SEI Techn. Rev.* (71): 78–82.

Schmidt, M. C. et al. (2007). Demonstration of *m*-plane InGaN/GaN laser diodes, *Jap. J. Appl. Phys.* 46: L190–L191.

Schmidt, M. C. et al. (2007a). High power and high external efficiency *m*-plane InGaN light emitting diodes, *Jap. J. Appl. Phys.* 46: L126–L128.

Schowalter, L. J. et al. (2006). Development of native, single crystal AlN substrates for device applications, *phys. stat. sol. (a)* 203: 1667âĂŞ1671.

Schowalter, L. J. et al. (2004). Fabrication of native, single-crystal AlN substrates, *IPAP Conf. Series* 4: 38–40.

Schubert, E. F. & Kim, J. K. (2005). Solid-state light sources getting smart, *Science* 308: 1274–1278.

Schubert, E. F. (2006). *Light-Emitting Diodes (2nd ed.)*, Cambridge University Press.

Schujman, B. S. & Schowalter, L. J. (2010). GaN-ready aluminum nitride substrates for cost-effective, very low dislocation density III-nitride LEDs, Crystal IS, Inc., Final Scientific/Technical Report DE-FC26-08-NT01578.

Schultz, T. (2010). Defect analysis of aluminum nitride, Dr. rer. nat. thesis, Technishen Universität, Berlin.

Sedhain, A. et al. (2009). The origin of 2.78 eV emission and yellow coloration in bulk AlN substrates, *Appl. Phys. Lett.* 95: 262104.

Segal, A. S. et al. (2009). Modeling analysis of AlN and AlGaN HVPE, *phys. stat. sol. (c)* 6: S329–332.

Segal, A. S. et al. (2000). On mechanisms of sublimation growth of AlN bulk crystals, *J. Crystal Growth* 211: 68.

Segal, A. S. et al. (2004). Surface chemistry and transport effects in GaN hydride vapor phase epitaxy, *J. Crystal Growth* 270: 384–395.

Segal, A. S. et al. 1999). Transport phenomena in sublimation growth of SiC bulk crystals, *Mater. Sci. Engineer.* B61–62: 40–43.

Senawiratne, J. et al. (2005). Raman, photoluminescence and absorption studies on high quality AlN single crystals, *phys. stat. sol. (c)* 2: 2774–2778.

Seol, D. J. et al. (2003). Computer simulation of spinodal decomposition in constrained films, *Acta Mater.* 51: 5173–5185.

Shealy, J. R. et al. (2002). An AlGaN/GaN high-electron mobility transistor with an AlN sub-bufer layer, *J. Phys.: Condens. Matter* 14: 3499–3509.

Shi, Y. et al. & Kuball, M. (2001). New technique for sublimation growth of AlN single crystals, *MRS Internet J. Nitride semicond. Res.* 6: 7.

Shur, M. S. (1998). GaN based transistors for high power applications, *Solid-State Electron.* 42: 2131–2138.

Sitar, Z. et al. (2004). Growth of AlN crystals by vaporization of Al and sublimation of AlN powder, *IPAP Conf. Series* 4: 41–45.

Skierbiszewski, C. (2005). From high electron mobility GaN/AlGaN heterostructures to blue-violet InGaN laser diodes. perspectives of MBE for nitride optoelectronics, *Acta Physica Polonia* 108: 635–651.

Skromme, B. et al. (2002). Optical characterization of bulk GaN grown by a Na-Ga melt technique, *J. Crystal Growth* 246: 299–306.

Slack, G. A. & McNelly, T. F. (1977). Growth of high purity AlN crystals, *J. Crystal Growth* 34: 263–279.

Slack, G. A. et al. (2002). Some effects of oxygen impurities on AlN and GaN, *J. Crystal Growth* 246: 287–298.

Slack, G. A. et al. (2004). Properties of crucible materials for bulk growth of AlN, *Mat. Res. Soc. Symp. Proc.* 798: Y10.74.

Song, Y. et al. (2004). Preparation and characterization of bulk GaN crystals, *J. Crystal Growth* 260: 327–330.

Song, Y. et al. (2003). Bulk GaN single crystals: growth conditions by flux method, *J. Crystal Growth* 247: 275–278.

Speck, J. S. (2001). The role of threading dislocations in the physical properties of GaN and its alloys, *Mater. Sci. Forum* 353-356: 769–778.

Speck, J. S. & Rosner, S. J. (1999). The role of threading dislocations in the physical properties of GaN and its alloys, *Physica B: Condensed Matter* 273-274: 24–32.

Srikant, V. et al. (1997). Mosaic structure in epitaxial thin films having large lattice mismatch, *J. Appl. Phys.* 82: 4286–4295.

Steckl, A. J. et al. (1997). Growth and characterization of GaN thin films on SiC SOI substrates, *J. Electron. Mater.* 26: 217 – 223.

STR-soft (2000). http://www.str-soft.com/products/Virtual_Reactor/.

Strassburg, M. et al. (2004). The growth and optical properties of large, high-quality AlN single crystals, *J. Appl. Phys.* 96: 5870–5876.

Stutzmann, M. et al. (2001). Playing with polarity, *phys. stat. sol. (b)* 228: 505–512.

Taguchi, T. (2003). Present status of white LED lighting technology in Japan, *J. Light & Vis. Env.* 27: 131–138.

Tamulatis, G. et al. (2003). Photoluminescence of GaN deposited on single-crystal bulk AlN with different polarities, *Appl. Phys. Lett.* 83: 3507–3509.

Tihonov, A. & Arsenin, V. (1977). *Solution of Ill-posed problems*, ISBN-10: 0470991240, ISBN-13: 978-0470991244, Wiley, New York.

Tomita, K. et al. (2004). Self-separation of freestanding GaN from sapphire substrates with stripe-shaped GaN seeds by HVPE, *IPAP Conf. Series* 4: 28–31.

Usikov, A. S. et al. (2003). Indium-free violet LEDs grown by HVPE, *phys. stat. solidi (c)* 0: 2265–2269.

Utsumi, W. et al. (2003). Congruent melting of gallium nitride at 6 GPa and its application to single crystal growth, *Nat. Mater.* 2: 735–738.

Vaudo, R. P. et al. (2003). Characteristics of semi-insulating Fe doped GaN substrates, *phys. stat. sol. (a)* 200: 18–21.

Vodakov, Y. A. et al. (2003). Tantalum crucible fabrication and treatment, US Patent 6,547,87.

Wadley, H. G. et al. (2001). Mechanisms, model and methods of vapor deposition, *Progr. Mater. Sci.* 46: 329–377.

Waldrip, K. E. (2007). Initial Exploration of Growth of InN by Electrochemical Solution Growth, SAND2010-0952, 20 pp.

Waldrip, K. E. (2007). Molten salt-based growth of bulk GaN and InN for substrates, SAND2007-5210, 27 pp.

Waltereit, P. et al. (2002). Heterogeneous growth of GaN on 6H-SiC (0001) by plasma-assisted molecular beam epitaxy, *phys. stat. sol. (a)* 194: 524–527.

Wang, C. et al. (2001). Influence of growth parameters on crack density in thick epitaxial lateral overgrown GaN layers by hydride vapor phase epitaxy, *J. Crysytal Growth* 230: 377–380.

Wang, T. C. et al. (2001a). Dislocation evolution in epitaxial multilayers and graded composition buffers, *Acta. Mater.* 49: 1599–1605.

Wang, X. et al. (2006). Powder sublimation and porosity evolution in sublimation crystal growth, AIAA 2006-3270.

Wellmann, P. et al. (2006). Modeling and experimental verification of SiC M-PVT bulk crystal growth, *Mater. Sci. Forum* 527–529: 75–78.

Weyers, M. et al. (2008). GaN substrates by HVPE, *Proc. of SPIE* 6910: 691001.

Wolfson, A. A. & Mokhov, E. N. (2010). Dependence of the growth rate of an AlN layer on nitrogen pressure in a reactor for sublimation growth of AlN crystals, *Semicond.* 44: 1383–1385.

Wu, B. et al. (2005). Design of an RF-heated bulk AlN growth reactor: Induction heating and heat transfer modeling, *Crystal Growth & Design* 5: 1491–1495.

Wu, B. et al. (2004). Application of flow-kinetics model to the PVT growth of SiC crystals, *J. Crystal Growth* 266: 303–312.

Wu, X. H. et al. (1996). Defect structure of metal-organic chemical vapor deposition-grown epitaxial (0001) GaN/Al$_2$O$_3$, *J. Appl. Phys.* 80: 3228 - 3237.

Wu, X. H. et al. (1998). Dislocation generation in GaN heteroepitaxy, *J. Crystal Growth* pp. 231–243.

Xi, Y. A. et al. (2006). Very high quality AlN grown on (0001) sapphire by metal-organic vapor phase epitaxy, *Appl. Phys. Lett* 89: 103106.

Xi, Y. A. et al. (2006a). AlGaN UV light-emitting diodes emitting at 340 nm grown on AlN bulk substrates, Proc. L. Eastman Conf. High Performance Devices, Cornell Univ., 54–55.

Xing, H. et al. (2001). Gallium nitride based transistors, *J. Phys.: Condens. Matter* 13: 7139–7157.

Yakimova, R. et al. (2005). Sublimation growth of AlN crystals: Growth mode and structure evolution, *J. Crystal Growth.* 281: 81–86.

Yamabe, N. et al. (2009). Nitridation of Si(1 1 1) for growth of 2H-AlN(0 0 0 1)/Si$_3$N$_4$ /Si(1 1 1) structure, *J. Crystal Growth*: 3049-3053.

Yamane, H. et al. (1998). Morphology and characterization of GaN single crystals grown in a Na flux, *J. Crystal Growth* 186: 8–12.

Yan, F. et al. (2007). High-efficiency GaN-based blue LEDs grown on nano-patterned sapphire substrates for solid-state lighting, *Proc. of SPIE* 6841: 684103.

Yano, M. et al. (2000). Growth of nitride crystals, BN, AlN and GaN by using a Na flux, *Diamond and Related Materials* 9: 512–515.

Yazdi, G. R. et al. (2006). Growth and morhology of AlN crystals, *Phys. Scr.* T126: 127–130.

Yonemura et al. (2005). Precipitation of single crystalline AlN from Cu-Al-Ti solution under nitrogen atmosphere, *J. Mater. Sci.: Mater. In Electron.* 16: 197–201.

Yoshikawa, A. et al. (2004). Crystal growth of GaN by ammonothermal method, *J. Crystal Growth* 260: 67–72.

Zheleva, T. et al. (1999). Pendeo-epitaxy - a new approach for lateral growth of gallium nitride films, *J. Electron. Mater.* 28: L5–L8.

Zhmakin, A. I. (2004). Heat transfer problems in crystal growth, Keynote lecture. 3rd Int. Symp. Adv. in Comp. Heat Transfer, 2004, Norway. CD Proc., Begell House, 24 pp.

Zhmakin, A. I. (2011a). Enhancement of light extraction from light-emitting diodes, *Phys. Reports* 498: 189–241.

Zhmakin, A. I. (2011b). Strain relaxation models, arXiv:1102.5000v1 [cond-mat.mtrl-sci].

Zhmakin, I. A. et al. (2000). Evolution of thermoelastic strain and dislocation density during sublimation growth of silicon carbide, *Diamond and Related Materials* 9: 446–451.

Zukauskas, A. et al. (2002). *Introduction to Solid State Lighting*, ISBN-10: 0471215740, ISBN-13: 978-0471215745, Wiley, New York.
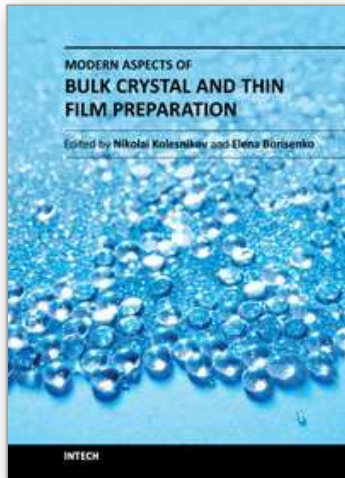
Modern Aspects of Bulk Crystal and Thin Film Preparation

Edited by Dr. Nikolai Kolesnikov

In modern research and development, materials manufacturing crystal growth is known as a way to solve a wide range of technological tasks in the fabrication of materials with preset properties. This book allows a reader to gain insight into selected aspects of the field, including growth of bulk inorganic crystals, preparation of thin films, low-dimensional structures, crystallization of proteins, and other organic compounds.

How to reference

In order to correctly reference this scholarly work, feel free to copy and paste the following:

O.V. Avdeev, T.Yu. Chemekova, E.N. Mokhov, S.S. Nagalyuk, H. Helava, M.G. Ramm, A.S. Segal, A.I. Zhmakin and Yu.N. Makarov (2012). Development of 2" AlN Substrates Using SiC Seeds, Modern Aspects of Bulk Crystal and Thin Film Preparation, Dr. Nikolai Kolesnikov (Ed.), ISBN: 978-953-307-610-2, InTech, Available from: http://www.intechopen.com/books/modern-aspects-of-bulk-crystal-and-thin-film-preparation/development-of-2-aln-substrates-using-sic-seeds

INTECH
open science | open minds